Palaeogeography, Palaeoclimatology, Palaeoecology 589 (2022) 110824

Contents lists available at ScienceDirect

Palaeogeography, Palaeoclimatology, Palaeoecology

journal homepage: www.elsevier.com/locate/palaeo

The exceptionally preserved Early Cretaceous "Moqi Fauna" from eastern Inner Mongolia, China, and its age relationship with the Jehol Biota

Zhiqiang Yu [a,b,c,1], Liping Dong [a,b,1], Magdalena H. Huyskens [d], Qing-Zhu Yin [d], Yuan Wang [a,b], Chenglong Deng [c], Huaiyu He [c,*]

[a] Key Laboratory of Vertebrate Evolution and Human Origin of Chinese Academy of Sciences, Institute of Vertebrate Paleontology and Paleoanthropology, Chinese Academy of Sciences, Beijing 100044, China
[b] CAS Centre for Excellence in Life and Paleoenvironment, Beijing 100044, China
[c] State Key Laboratory of Lithospheric Evolution, Institute of Geology and Geophysics, Chinese Academy of Sciences, Beijing 100029, China
[d] Department of Earth and Planetary Sciences, University of California at Davis, Davis, CA 95616, USA

ARTICLE INFO

Editor: Howard Falcon-Lang

Keywords:
Early Cretaceous
Moqi Fauna
Conservation lagerstätten
Geochronology

ABSTRACT

New fossil-bearing horizons at the Gezidong and Jiaxikou localities, eastern Inner Mongolia, referred to as the Moqi fossil bed, yield a diverse fossil assemblage coined herein as "Moqi Fauna". The Moqi Fauna provides important insights into the evolution of some vertebrate clades, such as frogs and salamanders, and their Early Cretaceous diversification. In this paper, we report an improved chronology of the Moqi fossil bed based on SIMS and high-precision CA-ID-IRMS U-Pb zircon analyses of three tuff samples from horizons that are interstratified with the fossil-bearing layer at two localities. The SIMS U-Pb dating method applied on zircons from three samples gave dates of 117.8 ± 0.9/1.5 Ma, 117.7 ± 1.0/1.5 Ma, and 118.3 ± 1.2/1.7 Ma, respectively. Two high-precision CA-ID-IRMS U-Pb weighted mean $^{206}Pb/^{238}U$ ages of, 119.20 ± 0.38/0.38/0.72 Ma and 118.67 ± 0.13/0.14/0.28 Ma were also obtained. These findings indicate the age of the Moqi Fauna is ca. 119.20 Ma to 118.67 Ma. Comparison of the Moqi Fauna with the well-known Jehol Biota, as well as the Fuxin Biota of a slightly younger age, suggests that the Moqi Fauna was a distinct fauna which shows a potential link with the Jehol Biota.

1. Introduction

Late Mesozoic terrestrial biotas in northern China, especially the Yanliao Biota from the Middle-Upper Jurassic Haifanggou and Tiaojishan formations, and the Jehol (sensu stricto) Biota from the Lower Cretaceous Huajiying, Yixian and Jiufotang formations, are extremely important assemblages. They contain numerous crucial fossils which shed new light on the evolution of various lineages (for example, plants see Sun et al., 1998, 2002; birds see Wang et al., 2018b; amphibians see Wang et al., 2007; mammals see Wang et al., 2019a) as well as some extinct clades (dinosaurs see Xu et al., 2003, 2020). They also provide rarely obtained information concerning the ecology and behavior of the ancient life forms (Xu and Norell, 2004; Evans and Wang, 2012; Hu et al., 2005).

In the last two decades, two new Early Cretaceous freshwater fossil localities, the Gezidong and Jiaxikou localities, from the Morin Dawa Daur Autonomous County (Moqi for short), eastern Inner Mongolia, China in the Dayangshu Basin, have drawn extensive attention among paleontologists with an increasing number of exceptionally preserved frogs, salamanders, fishes, and birds, as well as conchostracans and insects (Jia and Gao, 2016; Gao and Chen, 2017; Wang et al., 2019; Xing et al., 2019). Those fossils have been considered to be components of the Jehol Biota due to the coappearance of *Eosestheria* (conchostracan), *Ephemeropsis* (insect), and possible *Lycoptera* (fish) (EEL assemblage) at both localities. However, whether the fossil assemblage from the Moqi localities is a local representation of the Jehol Biota remains ambiguous due to (1) the long distance from the Yanliao area (northern Hebei, western Liaoning, and southeastern Inner Mongolia), the poor stratigraphic correlation, and more importantly the lack of precise age constraints; and (2) the equivocal or incorrect definition of the Jehol Biota (*sensu stricto*).

The fossil-bearing horizons of the Gezidong and Jiaxikou localities

* Corresponding author.
E-mail addresses: zhiqiangyu@mail.iggcas.ac.cn (Z. Yu), dongliping@ivpp.ac.cn (L. Dong), mhuyskens@ucdavis.edu (M.H. Huyskens), qyin@ucdavis.edu (Q.-Z. Yin), wangyuan@ivpp.ac.cn (Y. Wang), cldeng@mail.iggcas.ac.cn (C. Deng), huaiyuhe@mail.iggcas.ac.cn (H. He).
[1] These authors contributed equally: Zhiqiang Yu, Liping Dong.

https://doi.org/10.1016/j.palaeo.2021.110824
Received 13 October 2021; Received in revised form 29 December 2021; Accepted 29 December 2021
Available online 4 January 2022

have been taken as stratigraphically equivalent to the Yixian or Jiufotang Formation in the Yanliao area based on the same paleontological evidence (i.e., the appearance of the EEL assemblage) and the possible correlation with the Guanghua Formation or Longjiang Formation, which was dated to 125 Ma or 125–120 Ma (Jia and Gao, 2016; Gao and Chen, 2017; Xing et al., 2019). However, due to the restricted and scattered outcrops of Early Cretaceous volcano-sedimentary rocks and the lack of the stratigraphic work in the Dayangshu Basin and the adjacent basins, the fossil-bearing horizons have not been evidently correlated with the Guanghua or Longjiang formations in the Longjiang Basin, or the Jiufengshan Formation in the Dayangshu Basin (such as Naketa locality, Li and Reisz, 2020), not mentioning the Yixian or Jiufotang formations of the faraway Yanliao area. Moreover, although a date of 121.23 ± 0.74 Ma was reported (Wang et al., 2019), the LA-ICP-MS dating method used has large uncertainty and poor reproducibility, and precise dating to strictly constrain the horizon and its fossils is still lacking.

In this paper, we refer to the fossil-bearing layers of the Gezidong and Jiaxikou localities (together as Moqi localities) as the "Moqi fossil bed" of conservation lagerstätte (see below) and coin the fossil assemblage from the Moqi localities as the Moqi Fauna. We present SIMS (secondary ion mass spectrometry) and CA-ID-IRMS (chemical abrasion-isotope dilution isotope ratio mass spectrometry) U-Pb zircon dating of the Moqi fossil bed and Moqi Fauna and further discuss the relationship between the Moqi Fauna and the Jehol Biota.

2. Geological background

There are many Cretaceous continental rift basins and a massive amount of magmatic rocks in Northeast China due to crustal contraction and extension triggered by the subduction of the paleo-Pacific plate during the late Mesozoic (Ren et al., 2002; Wu et al., 2011; Meng et al., 2021). Among those rift basins, the Dayangshu Basin is located in the eastern part of the Great Xing'an Range, and stretches NE-SW for a distance of approximately 100 km and has a width of about 30 km (IMBGMR, 1991) (Fig. 1a). The Nenjiang-Balihan Fault separates the Dayangshu Basin in the northwest from the Songliao Basin in the southeast and controlled the formation and evolution of the Dayangshu Basin during the Mesozoic time.

The classification and lithostratigraphic divisions of the Early Cretaceous volcano-sedimentary successions in the Great Xing'an Range are highly disputed due to the complexity of non-marine strata, the weak geologic observations, and the fragmented geological records (Li et al., 2010; Li and Reisz, 2020). Within the Dayangshu Basin, the late Mesozoic terrestrial sedimentary sequence normally comprises the Lower Cretaceous Longjiang/Guanghua?, Jiufengshan and Ganhe formations, and the Upper Cretaceous Nenjiang Formation (Fig. 2) (IMBGMR, 1991).

2.1. Stratigraphy

The Longjiang Formation has been used by various researchers under different definitions (IMBGMR, 1991; HBGMR, 1993; 1997). The

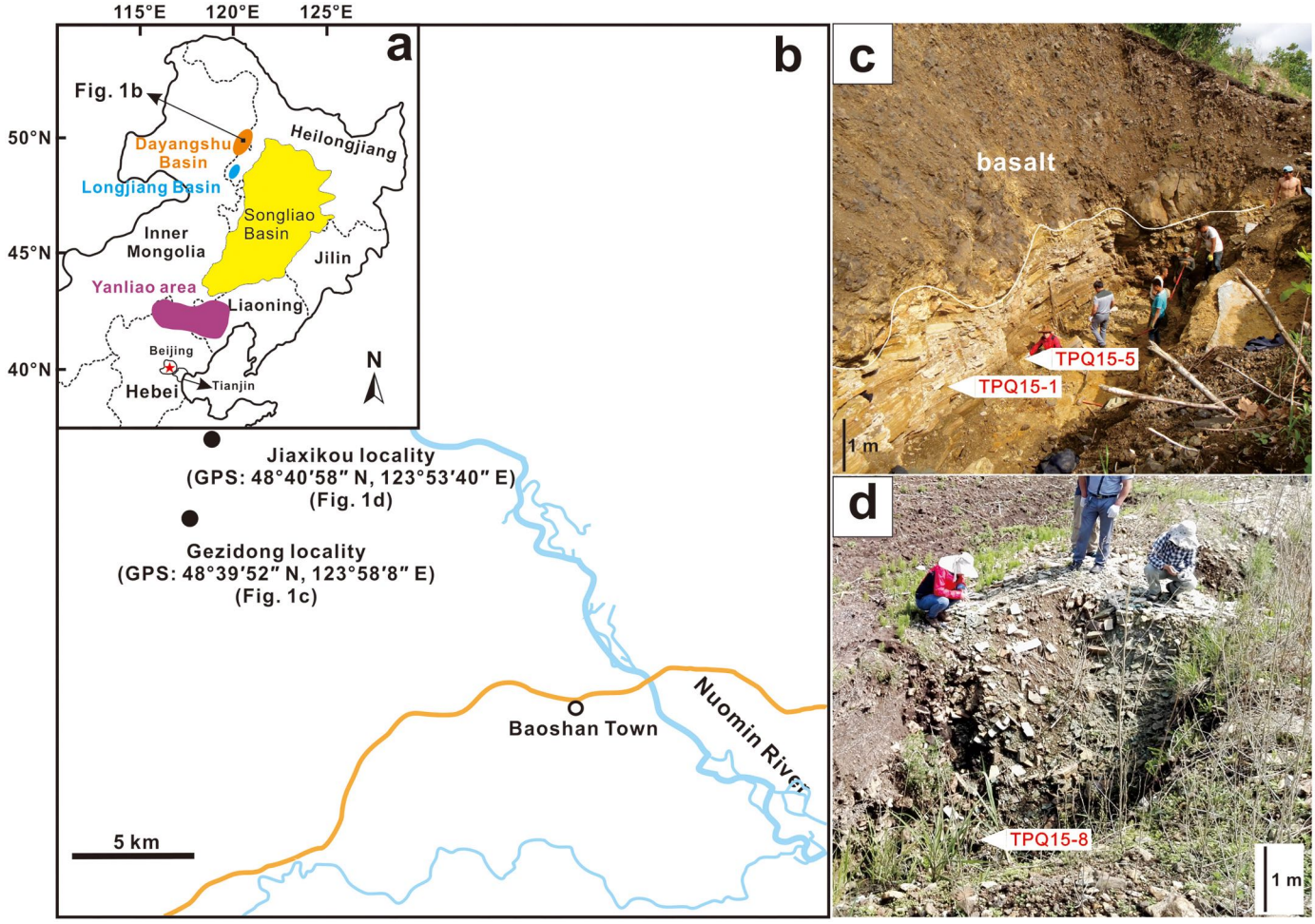

Fig. 1. (a) Schematic map showing the location of the study area in eastern China. (b) Geographic position of Gezidong and Jiaxikou fossil localities within the study area. Photos showing the Moqi fossil bed as well as the positions of the sampled tuff layers at the Gezidong (c) and Jiaxikou (d) fossil localities.

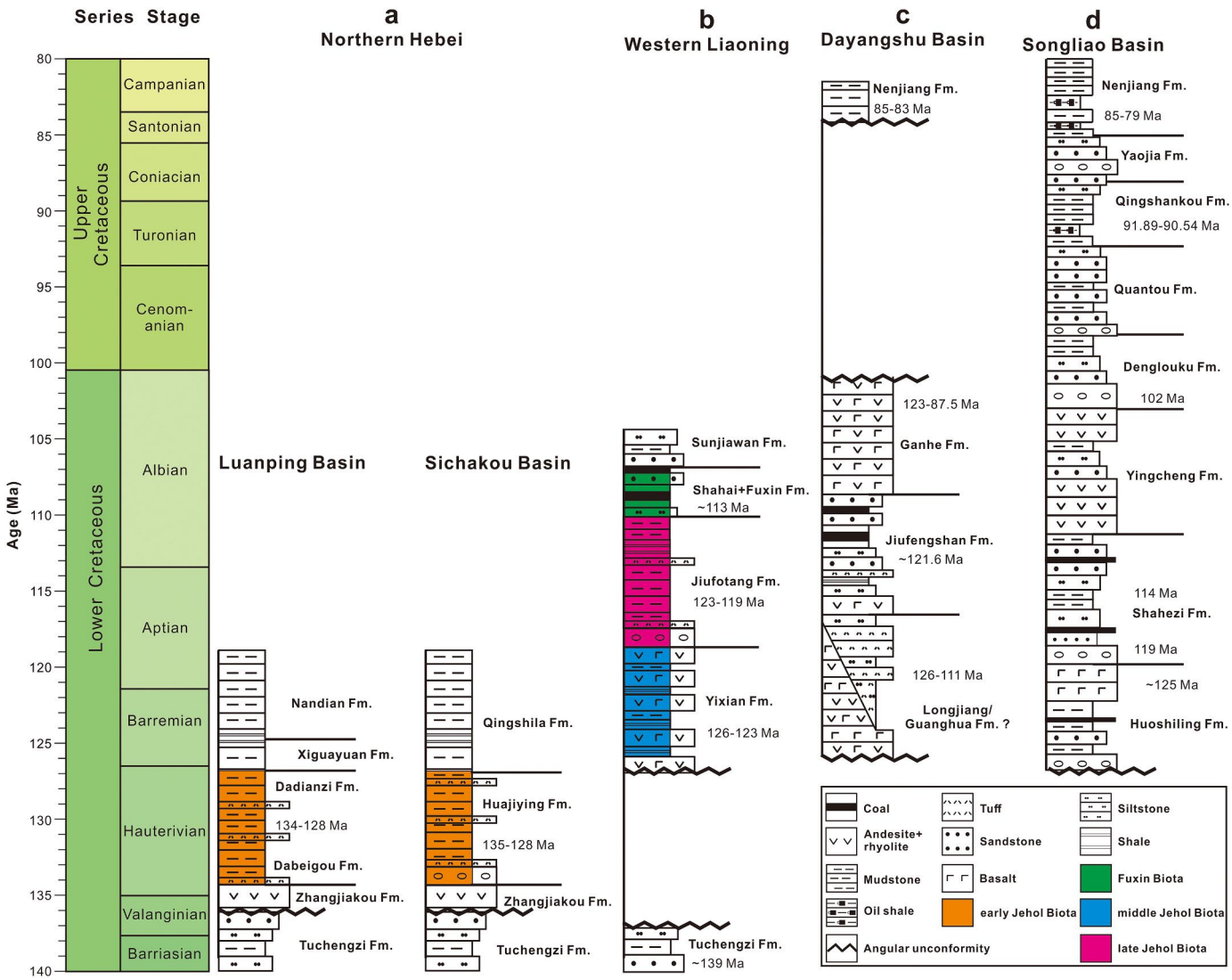

Fig. 2. Chronostratigraphy and lithostratigraphy of the Cretaceous non-marine strata mentioned in this study. (a) northern Hebei, (b) western Liaoning, (c) the Dayangshu Basin, and the adjacent Songliao Basin (d). Geologic time scale is from Gale et al. (2020).

holostratotype Shanquan section in Longjiang County, Heilongjiang (125°55′E, 47°14′N) within the Longjiang Basin, was firstly introduced by the First Regional Geological Survey Team of Inner Mongolia Autonomous region in 1972 (IMBGMR, 1991). This section composed mainly of intermediate-acid volcanic rocks interbedded with fossil-bearing sedimentary clastic rocks, was divided into the "middle Xing'an Range volcanic member" (the first ten layers) of mainly intermediate lava and the overlying "upper Xing'an Range volcanic member" characterized by acid volcanic rocks. The former was named as the "Longjiang Formation" in 1974 (Wang et al., 1997), i.e., Longjiang Formation *sensu strito* and the latter as "Guanghua Formation" in 1991 (IMBGMR, 1991).

A broader Longjiang Formation (*sensu lato*) was proposed in 1976 to include the "middle Xing'an Range volcanic member" (sensu *strito*) and the "upper Xing'an Range volcanic member" (Guanghua Formation) (IMBGMR, 1991). Although HBGMR (1997) and IMBGMR (1996) followed the broader Longjiang Formation, whether the Guanghua Formation should be treated separately is still highly debated (HBGMR, 1993; Ding et al., 2014) due to the different opinions on the nature of the contact between the two layers. Further investigation is needed to address this issue, however, it is beyond the scope of this study. Many radiometric dates with variable data quality from the Longjiang/Guanghua? Formation have been reported, ranging from 126.5 Ma to 110.7 Ma (Table 1).

The Jiufengshan Formation was first established in the Dayangshu coalfield in Oroqen Autonomous County, Inner Mongolia Autonomous Region by the Coal Management Bureau of the Heilongjiang Province in 1974, representing the coal-bearing strata in the Dayangshu Basin (HBGMR, 1997; Li, 2010). It was highly disputed whether the basalt occurred in the formation. The Jiufengshan Formation yields abundant fossils, including plants (*Zamites* sp., *Czekanowskia rigida*, *Pityophyllum lindstroemi*, *P. nordenskioldi*, *Cephalotaxopsis* sp., *Coniopteris* sp., *Ginko digitate*, *Podozamites lanceolatus*), spinicaudatans, spore and pollens (Wang et al., 1997). The Jiufengshan Formation at Naketa fossil locality was dated at 121.6 ± 0.5 Ma by zircon LA-ICP-MS dating (Li and Reisz, 2020).

The Ganhe Formation was derived from the term "Ganhe volcanic rocks" by Tan and Wang in 1929 (HBGMR, 1997), representing the basic volcanic rocks, pyroclastic rocks, and interbedded sedimentary rocks in the Ganhe river region. The holostratotype section of this formation was from the well #67–215 (124°35′E, 49°46′N) in Oroqen Autonomous County, Inner Mongolia Autonomous Region drilled in 1973 (IMBGMR, 1996). The age of the Ganhe Formation is bracketed between 123.1 Ma and 87.5 Ma (Table 1).

Table 1
Summary of geochronology of the Lower Cretaceous from Dayangshu Basin and its adjacent areas.

Sample	Location	GPS site	Lithostratigraphic Formation	Lithology	Age (Ma)	uncertainty (Ma)	Method	References
YL018	Shanquan	–	Longjiang	Rhyolite	125.4	1.8	Whole rock Ar–Ar	Ding et al., 2014
1581–2	Mohe	–	Guanghua	Rhyolite	125	2		
1579–5	Pangu	–	Guanghua	Rhyolite	126	2	LA-ICP-MS	Guo et al., 2015
1575–4	Walagan	–	Ganhe	Andesite	120	2	Zircon U-Pb	
1565–5	Cuigang	–	Ganhe	Andesite	122	4		
D3164	Xinsheng	50°33′12″N; 126°22′44″E	Longjiang	Rhyolite	120	1.3	Zircon U-Pb	Li et al., 2015b
PM02–74	Xinsheng	50°31′01″N; 126°28′17″E	Longjiang	Andesite	110.7	1.2	Zircon U-Pb	Li et al., 2015b
PM412TW25	Dajingshan	47°9′28″N; 122°56′27″E	Guanghua	Rhyolite	122.4	1.7	Zircon U-Pb	Zhang et al., 2017
YL004	Xujiatun	47°13′00″N; 122°57′38″E	Ganhe	Basalt	87.50	0.7	Whole rock Ar–Ar	Li et al., 2013b
YL052	Yaluhe	47°17′21″N; 123°04′20″E	Ganhe	Andesite	123.1	1.1	Whole rock Ar–Ar	Li et al., 2013b
YL018	Guanghuayidui	47°13′53″N; 122°57′38″E	Guanghua	Dacite	125.4	1.8	Whole rock Ar–Ar	Li et al., 2013b
YL046	Sanjiaosan	47°9′48″N; 122°56′16″E	Guanghua	Rhyolite	121.6	1.4	Whole rock Ar–Ar	Li et al., 2013b
YL049	Dongduibao	47°14′19″N; 123°04′38″E	Guanghua	Rhyolite	101.50	0.8	Whole rock Ar–Ar	Li et al., 2013b
YL008	Menggushan	47°15′27″N; 122°53′9″E	Guanghua	Rhyolite	117.0	9	Whole rock Ar–Ar	Li et al., 2013b
YL020	Shaojiawopeng	47°17′28″N; 122°41′18″E	Longjiang	Andesite	125.1	1.5	Whole rock Ar–Ar	Li et al., 2013b
YL008	Menggushan	47°15′27″N; 122°53′9″E	Guanghua	Rhyolite	126.5	1.1	Zircon U-Pb	Li et al., 2013a
YL018	Guanghuayidui	47°13′53″N; 122°57′38″E	Guanghua	Dacite	124.6	1.1	Zircon U-Pb	Li et al., 2013a
YL020	Shaojiawopeng	47°17′28″N; 122°41′18″E	Longjiang	Andesite	126.1	1.7	Zircon U-Pb	Li et al., 2013a
YL046	Sanjiaosan	47°9′48″N; 122°56′16″E	Guanghua	Rhyolite	122.2	1.1	Zircon U-Pb	Li et al., 2013a
SDP1414B	Sandaowanzi	–	Longjiang	Andesite	121.4	1.8	Zircon U-Pb	Wang et al., 2017b
SDP1431	Sandaowanzi	–	Longjiang	Andesite	122.0	1.1	Zircon U-Pb	Wang et al., 2017b
DGS07	Xinglong	–	Longjiang	Andesite	119	1	Zircon U-Pb	Deng et al., 2019
	Xinglong	–	Guanghua	Rhyolite	120	1	Zircon U-Pb	Deng et al., 2019
DGS05	Gezidong	–	–	Tuff	121.23	0.74	Zircon U-Pb	Wang et al., 2019
	Naketa	48°22′08.1″N; 123°12′50.9″E	Jiufengshan	Tuff	121.6	0.47	Zircon U-Pb	Li and Reisz, 2020
19 dB01–03	Ganhe	49°16′42.13″ N; 124°39′18.81″E	Gushanzhen (Ganhe)	Andesite	104	1	Zircon U-Pb	Zhang et al., 2020
19 dB04–07	Ganhe	49°16′39.08″ N; 124°39′16.53″E	Gushanzhen (Ganhe)	Tuffaceous sandstone	101.2	0.6	Zircon U-Pb	Zhang et al., 2020
TW14	Handahan Town	47°02′38″ N; 122°41′6″E	Longjiang	Andesite	125.9	1.5	LA-ICP-MS Zircon U-Pb	Zhang et al., 2018
D9225–1	Daheishan	50°34′26.4″ N; 124°26′2.4″E	Longjiang (previously named as Xinghuo)	Andesite	120	2.1	LA-ICP-MS Zircon U-Pb	Du et al., 2018
D9448	Eergeqi	–	Longjiang (previously named as Zhuangzhi)	Andesite	123.1	2.3	LA-ICP-MS Zircon U-Pb	

The Nenjiang Formation (85–79 Ma) rests unconformably over the Lower Cretaceous section of the basin. The Nenjiang Formation is characterized by the petroleum source and oil-rich rocks in the Daqing Oil Field, which is widely distributed in the Songliao Basin (Yu et al., 2019). The fossil-bearing strata of the Nenjiang Formation in the Dayangshu Basin is correlated to the first member of the Nengjiang Formation based on the biostratigraphic and palaeontologic studies (Sun et al., 2020; Zhang et al., 2020). It is consistent with the paleogeographic study of the Songliao Basin (Wang et al., 2013). During the first and second members of the formation, the paleo-Songliao lake expanded to the largest subaerial extent. The first member of the Nenjiang Formation is constrained between 85 Ma to 83 Ma (He et al., 2012; Deng et al., 2013; Yu et al., 2019).

2.2. The Gezidong and Jiaxikou fossil localities

The Gezidong (48°39′52″ N, 123°58′8″ E) and Jiaxikou (48°40′58″ N, 123°53′40″ E) fossil localities (Fig. 1b, c and d) are located northeast to the Baoshan Town, Morin Dawa Daur Autonomous County, Hulunbuir City, eastern Inner Mongolia, China. The exposed strata of these two fossil localities are mainly created from fossil excavations. The Gezidong section, about 10 m high, consists predominantly of volcano-sedimentary strata that can be subdivided into two parts: the lower fossil-bearing shales of approximately 2 m thick and the upper thick basalts (Fig. 1c and Fig. S1). The lithology of the Jiaxikou section is mainly shales of about 2 m thick (Fig. 1d).

The fossil-bearing layers of these two localities have been referred to the Guanghua Formation (126–101.5 Ma, Table 1) or Longjiang

Formation in various paleontological studies (Jia and Gao, 2016; Gao and Chen, 2017; Xing et al., 2019). However, as we stated previously, both Guanghua and Longjiang formations were named in the nearby but separate Longjiang Basin (HBGMR, 1993; Fig. 1a), and the lithological features at the Gezidong and Jiaxikou localities, such as the rock sequence and the nature of volcanic material, are different from those of Guanghua or Longjiang Formation. Therefore, the relationship between the fossil-bearing horizons at the Gezidong and Jiaxikou localities to Guanghua or Longjiang formations is not evident.

Li and Reisz (2020) referred the similar fossil-bearing strata in Dayangshu Basin to Jiufengshan Formation. However, the lithological nature of the fossil-bearing horizons at the Gezidong and Jiaxikou localities is also different from the Jiufengshan Formation at the Naketa locality (Li and Reisz, 2020). Further, there is no more evidence to

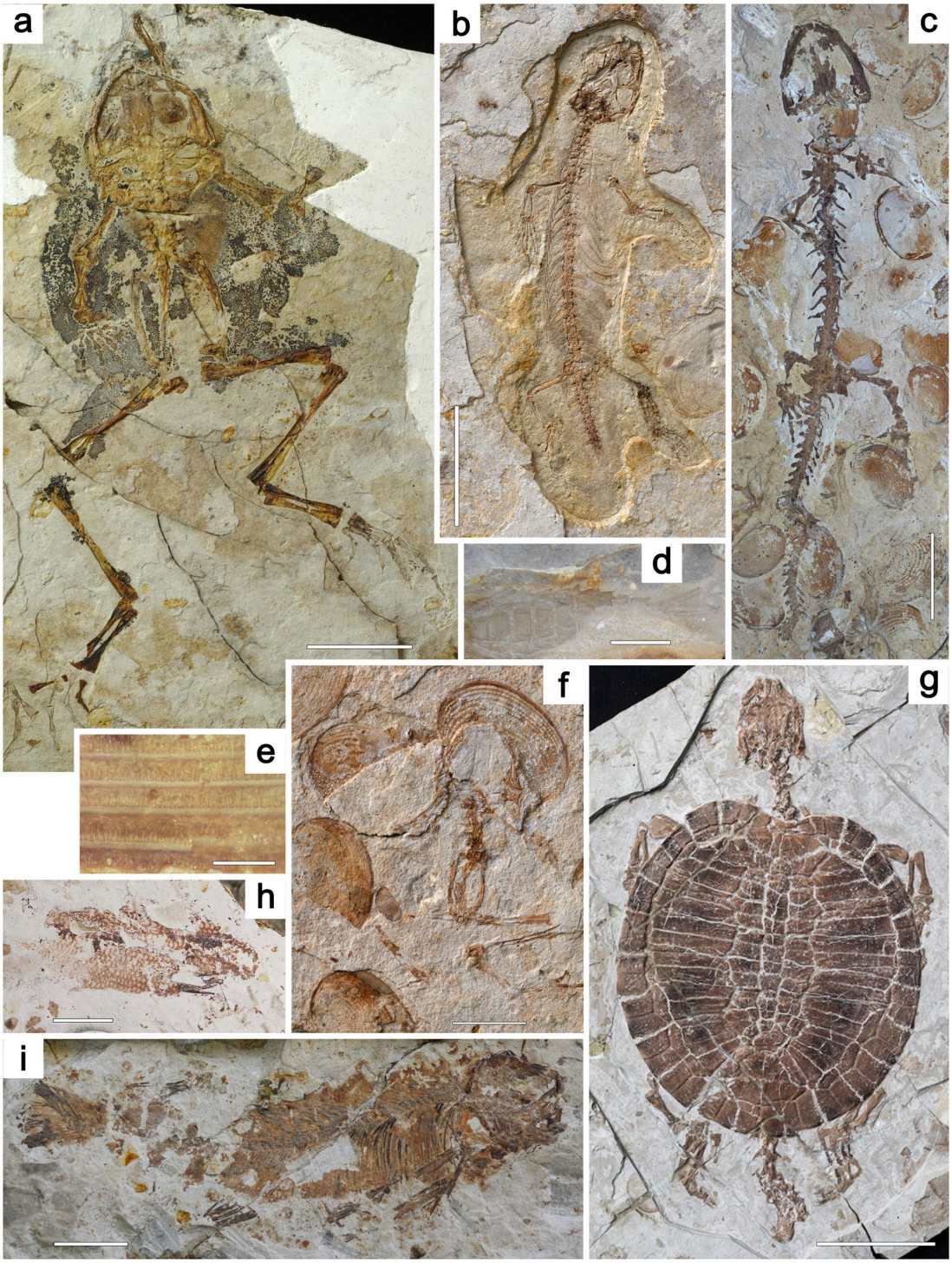

Fig. 3. Representatives of the Moqi Fauna and their preservational state. (a) An adult *Genibatrachus baoshanensis* skeleton with exceptionally preserved skin and eyes; (b) A complete skeleton of a small lizard (Squamata gen. et sp. nov.); (c) An adult *Nuominerpeton aquilonaris* skeleton; (d) Posterior part of the mayfly (*Ephemeropsis*); (e) ornamentation of the a conchostracon in detail; (f) A very young *Genibatrachus* skeleton with several conchostracons around it; (g) A complete macrobaenid skeleton in dorsal view; (h) Exquisitely preserved scales of a teleost; i) a *Jinanichthys* or *Lycoptera* skeleton with some scales preserved. The scale is 20 mm in (a), (b), (c) and (i), 10 mm in (d), (f) and (h), 0.5 mm in (e), and 50 mm in (g).

support the reference of the fossil-bearing horizons at the Gezidong and Jiaxikou localities to Jiufengshan Formation except for the presence of EEL assemblage. To be strict and more importantly to facilitate the future and more precise stratigraphic correlation, we use neither Guanghua (or Longjiang) Formation nor Jiufengshan Formation herein, but informally refer to the fossil-bearing horizons at the Gezidong and Jiaxikou localities as "Moqi fossil bed".

3. The Moqi Fossil Lagerstätte and Moqi Fauna

The Gezidong and Jiaxikou fossil localities intrigue extensive attention not only because of the extremely abundant frog fossils and an increasing level of diversity, but also due to the exceptional preservation of the fossils. The invertebrate fossils of mainly conchostracons and insects show clear and fine structures and the vertebrate fossils, of either frogs or turtles, are represented by mostly intact and fully articulated skeletons (Fig. 3).

Some of the frog fossils display exquisite preservation of skin and eyes (Fig. 3a), and one of the rare fish fossils (a teleost) preserves some continuous and overlapping scales of a teleost (Fig. 3h and i). Such exceptional preservation suggests the Moqi fossil bed is a conservation Lagerstätte, one of the two exceptional preservation types of Jehol Biota (Type A, Pan et al., 2013). This type of preservation could provide the information of the organisms that are not usually preserved in fossils, and therefore potentially present a comprehensive picture of the then ecosystem.

3.1. Biota (Fauna) in paleontological context

The Early Cretaceous Jehol Biota has long been defined by the EEL assemblage (Chen, 1988; Chang et al., 2003; Zhou et al., 2003), which is a biostratigraphic definition. There is neither a good nor a practical way to define Jehol Biota, even in the biostratigraphic context. As discussed in Pan et al. (2013), *Lycoptera* is restricted in the Yixian Formation and the fishes from Jiufotang Formation should be reassigned to *Jinanichthy*, which suggests the EEL assemblage does not occur in Jiufotang Formation. The same problem occurs to the '*Ephemeropsis*' from Yixian and Jiufotang formations. Therefore, the three key elements do not well represent the Jehol Biota.

In the context of the evolution of a biota, a biostratigraphic assemblage is far from a good definition. To understand the spatiotemporal distribution and evolutionary history of the Jehol Biota and its relationship to the contemporary biomes, Pan et al. (2013) proposed a paleoecological definition integrating the ecological and taphonomic aspects, which we follow in this study. Thus, the Jehol Biota consists of fossils from the Huajiying, the Yixian and Jiufotang formations in northern Hebei, western Liaoning, and southeast Inner Mongolia, in which volcanic and volcaniclastic beds are commonplace (Jiang et al., 2014; Rogers et al., 2015; Zhou et al., 2021), representing early, middle, and late stages of the biota, respectively. The fossils from other geological units and other areas should be treated separately. This leaves the relation between two biotas or faunas open, rather than just lumping everything together.

3.2. The Moqi Fauna

The fossils from the Moqi fossil bed at the Gezidong and Jiaxikou localities include conchostracons, insects, fishes, frogs, salamanders, turtles, lizards, birds, and dinosaurs, and herein we coin this diverse fossil assemblage, so far mostly of animal fossils, as "Moqi Fauna".

The invertebrates so far are mainly conchostracans (Fig. 3e and f), probably of a *Eosestheria* fauna component preserved clustered, with much rarer *Ephemeropsis*. The *Eoestheria* fauna lasted from the Hauterivian Dadianzi Formation to the Aptian Jiufotang Formation (Li et al., 2007) and distributed widely in north and northeast China, Mongolia, and the Transbaikal region, including the Yanliao area. There are possibly other insects and spiders (Wang et al., 2017a).

The fish fossils are surprisingly rare in the Moqi Fauna, considering the high occurrence of vertebrate fossils. These fishes include *Peipiaosteus* and possibly *Jinanichthys* (or *Lycoptera*?). These fishes are also present in the Jehol Biota and in the Early Cretaceous of adjacent regions.

The frogs, referred to a single species *Genibatrachus baoshanensis* (Gao and Chen, 2017) are abundant and represent individuals from late metamorphosed youngs to large and fully grown adults (Fig. 3a, f). This provides a unique opportunity in the world to study the ontogeny of a fossil frog from the Early Cretaceous in detail, such as the ossification sequence of the carpals in *Genibatrachus* (Roček et al., 2022). Many specimens of the salamander *Nouminerpeton aquailonaris* (Fig. 3c) were recovered together with frogs but much fewer in number than the frogs. They are also of different ontogenetic stages (Jia and Gao, 2016). A rare inter-amphibian predation was reported from Gezidong locality with a complete and articulated adult salamander skeleton of *Nouminerpeton* found within the body cavity of the frog *Genibatrachus* (Xing et al., 2019).

Frogs and salamanders are also abundant in Jehol Biota and much more diverse. There are four species of a single genus *Liaobatrachus* from the Yixian Formation (Dong et al., 2013) and unnamed but distinct specimens from the Jiufotang Formation (Wang et al., 2007; Dong, 2012). The Jehol salamanders also include four named species, namely *Laccotriton*, *Sinerpeton*, *Regalerpeton*, and *Liaoxitriton zhongjiani* (Wang and Evans, 2006; Zhang et al., 2009). It has never been reported that the Jehol frogs and salamanders occur together, although there are quite many frog and salamander fossil sites in Yanliao area.

An advanced ornithuromorph bird, *Khinganornis hulunbuirensis* was described (Wang et al., 2021a), and additionally, Wang et al. (2017c) showed another bird specimen in their figure that might be different from *Khinganornis* but they did not describe or name it. To the best of our knowledge, birds are abundant in Jehol Biota, comprising the two main clades (Ornithuromorpha and Enantiornithes) plus some basal taxa (Zhou and Wang, 2017). The Jehol ornithuromorphans are diverse, with more than twenty species named.

Wang et al. (2017c) also briefly mentioned other vertebrates, such as dinosaurs (Ornithopoda, small theropods) and turtles. We also found dozens of turtle specimens (Fig. 3g), representing a new genus and species of Macrobaenidae and showing a different combination of morphological features from macrobaenids of other Early Cretaceous localities of Northeast China. The newly excavated squamate material is a small lizard (Fig. 3b) and different from those of the Jehol Biota, representing a new species (Fig. 3b). The turtle and lizard fossils are now under study.

4. The age of the Moqi Fauna

4.1. Samples

Three tuff samples, TPQ15–5 and TPQ15–1 from the Gezidong section and TPQ15–8 from the Jiaxikou section, were collected for SIMS and CA-ID-IRMS U-Pb dating (see Fig. 1c and d for the positions of the samples). TPQ15–5 was collected from a yellowish-white tuff layer (about 3 cm thick) of the Gezidong section, TPQ15–1 from a grayish-yellow tuff layer (about 10 cm thick) that is slightly higher in stratigraphic section, and TPQ15–8 from a white tuff layer of the Jiaxikou section. The horizons where tuff samples are from contain a variety of vertebrate fossils. All the samples are dominantly composed of crystal pyroclasts and altered vitric fragments (Fig. S2).

4.2. U-Pb zircon geochronology

Zircons were separated out using conventional magnetic and heavy-liquid methods before hand-picking under a binocular microscope. Recovered zircon grains together with zircon standards Plěsovice

(Sláma et al., 2008) and Qinghu (Li et al., 2013) were mounted in epoxy discs and polished to expose the longitudinal section of crystals for analysis. Secondary ion mass spectrometry (SIMS) U-Pb analysis of zircons in the samples was conducted using the Cameca IMS-1280HR at the Guangzhou Institute of Geochemistry, Chinese Academy of Sciences. The procedures follow Li et al. (2009) and Li et al. (2010).

To address the age difference not only between two fossil localities in eastern Inner Mongolia but also to compare with the previous geochronological data from the Jehol Biota in the Yanliao area, high-precision U-Pb geochronology of the tuff beds TPQ15–5 and TPQ15–8 by the CA-ID-IRMS method was performed to produce a series of accurate and precise dates.

The chemical abrasion procedure is modified from Mattinson (2005), which is adapted for single zircon grains with temperature and time durations for annealing and leaching determined by Huyskens et al. (2016). Zircon grains were annealed at 900 °C and subsequently unpolished grains were analyzed by laser ablation ICP-MS (inductively coupled plasma mass spectrometry) for U-Pb geochronology (Table 3 and Fig. S3). These analyses are only used as a guide to identify any detrital or inherited components and to select the youngest population of zircons for the CA-ID-IRMS at the University of California Davis and are not intended for publication. No discussion or conclusions will be drawn from this data. The analyses confirmed a single age population, with the exception of one detrital grain out of 50 analyzed in sample TPQ15–8 of ~2 Ga. Subsequent to laser ablation analyses, selected grains were leached for 15 h at 190 °C, and a ^{202}Pb-^{205}Pb-^{233}U-^{236}U tracer (Huyskens et al., 2016) was added to the chemically abraded zircons prior to dissolution. Pb and U were separated from the matrix elements by standard HCl ion exchange chemistry and Pb was loaded onto zone refined Re filaments with a silica gel activator (Huyskens et al., 2012). Pb was analyzed on a Triton Plus TIMS (thermal ionization mass spectrometer) in peak jumping mode on a secondary electron multiplier. U isotope dilution measurements were performed on a Neptune Plus MC-ICP-MS (multi collector inductively coupled plasma mass spectrometer) using an ESI APEX introduction system. More details on the analytical methods can be found in Liao et al. (2020). In this study, Uranium isotopes are analyzed using the MC-ICP-MS method since it typically achieves a higher ion yield (here defined as detected ions/total atoms) compared to the traditional method of measuring UO_2^+ on a TIMS and thus having the potential for achieving higher

Table 2
SIMS U-Pb zircon analyses.

Sample/spot	[U] (ppm)	[Th] (ppm)	Th/U (meas)	f_{206}%	$^{207}Pb/^{235}U$	±σ (%)	$^{206}Pb/^{238}U$	±σ (%)	ρ	$^{207}Pb/^{235}U$	±σ	$^{206}Pb/^{238}U$	±σ
TPQ15–5@1	58	61	1.051	1.18	0.111	7.10	0.0177	1.67	0.24	107.2	7.3	113.1	1.9
TPQ15–5@2	90	120	1.324	1.76	0.119	7.57	0.0185	1.71	0.23	113.8	8.2	118.1	2.0
TPQ15–5@3	483	759	1.571	0.19	0.128	1.96	0.0193	1.50	0.76	122.3	2.3	123.2	1.8
TPQ15–5@4	83	119	1.430	0.47	0.122	2.88	0.0181	1.61	0.56	116.6	3.2	115.9	1.8
TPQ15–5@5	111	176	1.576	0.75	0.115	4.48	0.0183	1.58	0.35	110.5	4.7	117.0	1.8
TPQ15–5@6	70	86	1.223	0.47	0.122	4.41	0.0188	1.52	0.34	116.7	4.9	119.9	1.8
TPQ15–5@7	57	58	1.005	0.70	0.131	5.23	0.0184	1.66	0.32	124.8	6.2	117.5	1.9
TPQ15–5@8	71	95	1.328	0.55	0.126	5.26	0.0182	1.61	0.31	120.2	6.0	116.4	1.9
TPQ15–5@9	78	92	1.175	0.25	0.124	3.72	0.0186	1.60	0.43	119.0	4.2	118.6	1.9
TPQ15–5@10	81	109	1.343	0.45	0.126	3.85	0.0183	1.54	0.40	120.4	4.4	117.1	1.8
TPQ15–5@11	93	122	1.313	0.58	0.126	4.35	0.0188	1.63	0.38	120.6	5.0	120.3	1.9
TPQ15–5@12	56	56	0.998	1.25	0.115	9.39	0.0183	1.67	0.18	110.9	9.9	117.2	1.9
TPQ15–5@13	49	43	0.877	0.83	0.122	6.20	0.0185	1.64	0.26	117.2	6.9	118.5	1.9
TPQ15–5@14	76	69	0.907	0.40	0.127	4.73	0.0183	1.77	0.37	121.1	5.4	116.9	2.1
TPQ15–5@15	101	89	0.875	0.70	0.117	5.00	0.0181	1.50	0.30	112.4	5.3	115.9	1.7
TPQ15–1@01	51	48	0.942	0.21	0.127	5.9	0.0186	1.77	0.30	121.3	6.8	119.0	2.1
TPQ15–1@02	59	43	0.721	0.87	0.126	5.4	0.0180	1.59	0.29	120.1	6.1	114.8	1.8
TPQ15–1@03	38	49	1.293	0.75	0.122	7.7	0.0182	1.72	0.22	116.8	8.6	116.4	2.0
TPQ15–1@04	57	34	0.608	0.85	0.122	5.7	0.0191	1.83	0.32	116.7	6.3	121.8	2.2
TPQ15–1@06	48	60	1.247	1.39	0.138	5.1	0.0190	1.77	0.35	131.3	6.3	121.3	2.1
TPQ15–1@07	63	82	1.301	1.07	0.131	3.2	0.0190	1.78	0.55	125.4	3.8	121.3	2.1
TPQ15–1@08	57	72	1.250	0.98	0.132	3.9	0.0185	1.66	0.42	125.8	4.7	118.5	1.9
TPQ15–1@10	44	62	1.404	1.50	0.130	5.7	0.0181	1.70	0.30	124.4	6.6	115.6	1.9
TPQ15–1@11	55	74	1.341	0.81	0.119	5.9	0.0186	1.63	0.28	114.4	6.4	118.8	1.9
TPQ15–1@12	48	65	1.334	2.99	0.119	10.7	0.0186	1.65	0.15	114.5	11.6	118.7	1.9
TPQ15–1@13	50	57	1.122	1.27	0.106	7.6	0.0183	1.62	0.21	102.7	7.5	117.2	1.9
TPQ15–1@05	183	212	1.160	1.00	0.133	2.1	0.0196	1.52	0.71	126.4	2.6	124.9	1.9
TPQ15–1@09	34	29	0.837	75.08	1.041	28.1	0.0255	3.08	0.11	724.6	157.0	162.6	4.9
TPQ15–8@2	55	49	0.882	1.74	0.122	10.5	0.0186	1.77	0.17	117.1	11.6	119.1	2.1
TPQ15–8@3	36	39	1.075	0.77	0.119	8.86	0.0187	1.72	0.19	113.8	9.6	119.3	2.0
TPQ15–8@4	40	40	0.992	1.84	0.103	11.5	0.0182	1.73	0.15	99.6	11.0	116.3	2.0
TPQ15–8@5	36	40	1.096	1.03	0.114	8.48	0.0182	1.73	0.20	110.0	8.9	116.0	2.0
TPQ15–8@6	50	62	1.246	1.35	0.113	7.69	0.0184	1.86	0.24	108.6	8.0	117.6	2.2
TPQ15–8@7	49	64	1.306	0.84	0.129	3.39	0.0189	1.67	0.49	123.1	3.9	120.5	2.0
TPQ15–8@8	49	56	1.145	0.56	0.128	4.11	0.0184	1.72	0.42	122.6	4.8	117.3	2.0
TPQ15–8@9	59	70	1.191	0.93	0.129	4.81	0.0189	1.77	0.37	123.1	5.6	120.9	2.1
TPQ15–8@10	117	72	0.621	0.29	0.128	3.39	0.0184	1.57	0.46	122.1	3.9	117.7	1.8
TPQ15–8@11	48	57	1.196	1.28	0.127	3.57	0.0185	1.78	0.50	121.2	4.1	118.2	2.1
TPQ15–8@12	54	50	0.939	0.92	0.110	6.80	0.0178	1.65	0.24	105.9	6.9	114.0	1.9
TPQ15–8@13	64	91	1.432	0.53	0.126	3.89	0.0187	2.08	0.53	120.5	4.4	119.5	2.5
TPQ15–8@14	107	116	1.085	0.45	0.119	3.89	0.0182	1.59	0.41	114.5	4.2	116.5	1.8
TPQ15–8@15	89	154	1.720	1.03	0.111	7.27	0.0182	1.57	0.22	106.9	7.4	116.2	1.8
TPQ15–8@16	32	31	0.976	1.49	0.135	4.48	0.0189	1.83	0.41	129.0	5.4	120.9	2.2
TPQ15–8@17	78	113	1.455	0.65	0.130	3.02	0.0186	1.87	0.62	124.2	3.5	118.8	2.2
TPQ15–8@18	68	99	1.464	1.05	0.128	3.27	0.0184	1.59	0.49	122.1	3.8	117.3	1.8
TPQ15–8@19	52	56	1.084	1.33	0.114	7.26	0.0183	1.64	0.23	109.9	7.6	116.7	1.9
TPQ15–8@20	31	25	0.815	1.49	0.112	12.5	0.0183	1.76	0.14	108.1	12.9	117.1	2.0
TPQ15–8@1	48	47	0.982	8.65	0.086	38.48	0.0187	1.67	0.04	83.9	31.5	119.4	2.0

precision for the same amount of material. The ion yield for UO_2^+ analyses using a silica gel activator on Re filaments, which is the traditional method, has been reported between 0.2 and 0.5% (Yokoyama et al., 2001), whereas the ion yield for U^+ in a ICP-MS is typically around 1–1.5%, but has been reported to be up to 3% (Albarède et al., 2015; Chiang et al., 2019). In addition, no correction for oxide interference is necessary when measuring metallic U^+ on an ICP-MS as opposed to UO_2^+ by TIMS. The drawback to using MC-ICP-MS compared to TIMS measurements are the larger isotopic fractionation, which is monitored in real time using the double U spike IRMM 3636 and corrected (Verbruggen et al., 2008). To monitor for the accuracy of the results, the Temora reference zircon is processed with every sample batch. Together with the samples reported in this work, two Temora grains were analyzed and a weighted mean $^{206}Pb/^{238}U$ age of 417.55 Ma ± 0.15 Ma (MSWD = 0.078) was obtained. While this reference material is a naturally occurring zircon and shows some variations, the obtained date is within the range of previously reported dates (Schaltegger et al., 2021; von Quadt et al., 2016). The SIMS and CA-ID-IRMS U-Pb zircon geochronology analytical results are listed in Tables 2 and 3, respectively.

4.3. Analytical results

The SIMS and CA-ID-IRMS U-Pb zircon geochronology analytical results are listed in Tables 2 and 3, respectively. We report three levels of uncertainty for the CA-ID-IRMS age data, representing analytical uncertainty only as 95% confidence (X), analytical and tracer calibration uncertainties (Y), and analytical and tracer and decay constant uncertainties (Z), respectively (Villa et al., 2016). For U-Pb age comparison within the same laboratory, the first uncertainty is sufficient. The second uncertainty was used to compare U-Pb dates across different laboratories. When comparing dates across different methods (e.g., U-Pb vs. Ar-Ar dates), the third uncertainty should be used. For SIMS zircon U-Pb ages, we report two levels of uncertainty: Age ± X/Y, where X represents the analytical error, the error Y represents the analytical error plus external reproducibility (2SD; 1%), and it is approximately equal to error Z.

4.3.1. SIMS zircon U-Pb analyses

Most zircons from the sample TPQ15–5 are 35–120 μm in length and have aspect ratio between 1:1 and 1:3. Fifteen zircon grains were analyzed from sample TPQ15–5, U and Th contents are within the range 49–483 ppm and 43–759 ppm, respectively, with Th/U ratios of 0.875–1.576. Values for f_{206} (the proportion of common ^{206}Pb in total measured ^{206}Pb) are mostly lower than 1% (Table 2). Fifteen analyses from this sample yielded a weighted mean $^{206}Pb/^{238}U$ age of 117.7 ± 1.0/1.5 Ma (MSWD = 1.6) (Fig. 4a).

Most zircons from the sample TPQ15–1 are 30–90 μm in length and have aspect ratio between 1:1 and 1:2.5. Thirteen zircon grains were analyzed from sample TPQ15–1, U and Th contents are within the range 38–63 ppm and 34–82 ppm, respectively, with Th/U ratios of 0.608–1.404. Values for f_{206} are mostly lower than 2%. Eleven of these yields a concordia age of 118.2 ± 1.2 Ma and a weighted mean $^{206}Pb/^{238}U$ age of 118.3 ± 1.3/1.7 Ma (MSWD = 1.6) (Fig. 4b). The remaining two analyses yield older ages, indicative to xenocrysts (spots 5 and 9, Table 2).

Most zircons from the sample TPQ15–8 are 35–120 μm in length and have aspect ratio between 1:1 and 1:2. Nineteen zircon grains were analyzed from sample TPQ15–8, U and Th contents are within the range 31–117 ppm and 25–154 ppm, respectively, with Th/U ratios of 0.621–1.720. Values for f_{206} are mostly lower than 1% (Table 2). Nineteen analyses obtained a weighted mean $^{206}Pb/^{238}U$ age of 117.8 ± 0.9/1.5 Ma (MSWD = 0.82) (Fig. 4c). Those weighted mean ages are interpreted to be the crystallizing age of zircons, which can be used to constrain the lower limit age of the tuff beds.

4.3.2. CA-ID-IRMS zircon U-Pb analyses

Five zircon grains from sample TPQ15–5 and four zircon grains from sample TPQ15–8 were analyzed by CA-ID-IRMS, respectively. For sample TPQ15–5, one grain yields an older age of 123.80 Ma, suggesting a xeno- or antecrystic origin, and the remaining four analyses yield a weighted-mean $^{206}Pb/^{238}U$ age of 118.67 ± 0.13/0.14/0.28 Ma (n = 4, MSWD = 0.63) (Fig. 4d).

Out of four analyses of TPQ15–8, three are concordant, overlap within uncertainty and yield a weighted-mean $^{206}Pb/^{238}U$ age of 119.20 ± 0.38/0.38/0.46 Ma (n = 3, MSWD = 0.20) (Fig. 4e and f). The fourth analysis has a high Pb_c/Pb^* (common Pb/radiogenic Pb) ratio and is slightly discordant and is thus excluded from the weighted mean calculations even though the $^{206}Pb/^{238}U$ age does agree with other three dates. All zircons had low Pb* (<1.5 pg) content, which reduced the precision (Table 3).

Table 3
CA-ID-IRMS U-Pb zircon analyses.

Sample	Th	Compositional Parameters		Radiogenic Isotope Ratios						Isotopic Ages			
		Pb*	Pbc	206Pb	207Pb		206Pb		corr.	207Pb		206Pb	
	U	Pbc	(pg)	204Pb	235 U	% err	238 U	% err	coef.	235 U	±	238 U	±
	(a)	(b)	(b)	(c)	(d)	(e)	(f)	(e)		(f)	(e)	(f)	(e)
TPQ15–8@11	1.250	2.6	0.48	150	0.1273	8.8526	0.0186	0.5824	0.936	121.68	10.15	119.03	0.69
TPQ15–8@12	1.049	0.9	1.38	62	0.1499	12.8278	0.0188	0.8640	0.947	141.82	16.98	119.98	1.03
TPQ15–8@13	1.164	3.2	0.34	185	0.1245	9.5978	0.0187	0.6224	0.973	119.11	10.79	119.34	0.74
TPQ15–8@14	1.191	3.0	0.44	174	0.1231	8.4112	0.0187	0.5325	0.953	117.91	9.36	119.24	0.63
TPQ15–5@1	1.006	3.7	0.47	220	0.1289	5.9199	0.0194	0.3838	0.892	123.07	6.86	123.80	0.47
TPQ15–5@2	1.163	2.6	0.49	153	0.1208	8.7524	0.0185	0.5525	1.091	115.84	9.58	118.26	0.65
TPQ15–5@3	1.262	3.4	0.31	195	0.1237	9.8360	0.0186	0.6430	1.105	118.39	10.99	118.72	0.76
TPQ15–5@4	2.203	12.7	0.60	557	0.1234	1.8003	0.0186	0.1191	1.044	118.12	2.01	118.69	0.14
TPQ15–5@5	1.638	5.2	0.41	262	0.1238	5.4256	0.0186	0.3553	1.092	118.53	6.07	118.62	0.42

(a) Model Th/U ratio calculated from radiogenic $^{208}Pb/^{206}Pb$ ratio and $^{207}Pb/^{235}U$ age.
(b) Pb* and Pb_c represent radiogenic and common Pb, respectively.
(c) Measured ratio corrected for spike and fractionation only.
(d) Corrected for fractionation, spike, and common Pb; all common Pb was assumed to be blank with the isotopic composition of $^{206}Pb/^{204}Pb$ = 18.59 ± 0.65%; $^{207}Pb/^{204}Pb$ = 15.79 ± 0.70%; $^{208}Pb/^{204}Pb$ = 38.54 ± 0.65% (1σ).
(e) Errors are 2-sigma, propagated using the algorithms of Schmitz and Schoene (2007) and Crowley et al. (2007).
(f) Calculations are based on the decay constants of Jaffey et al. (1971) and a $^{238}U/^{235}U$ ratio of 137.818 (Hiess et al., 2012).

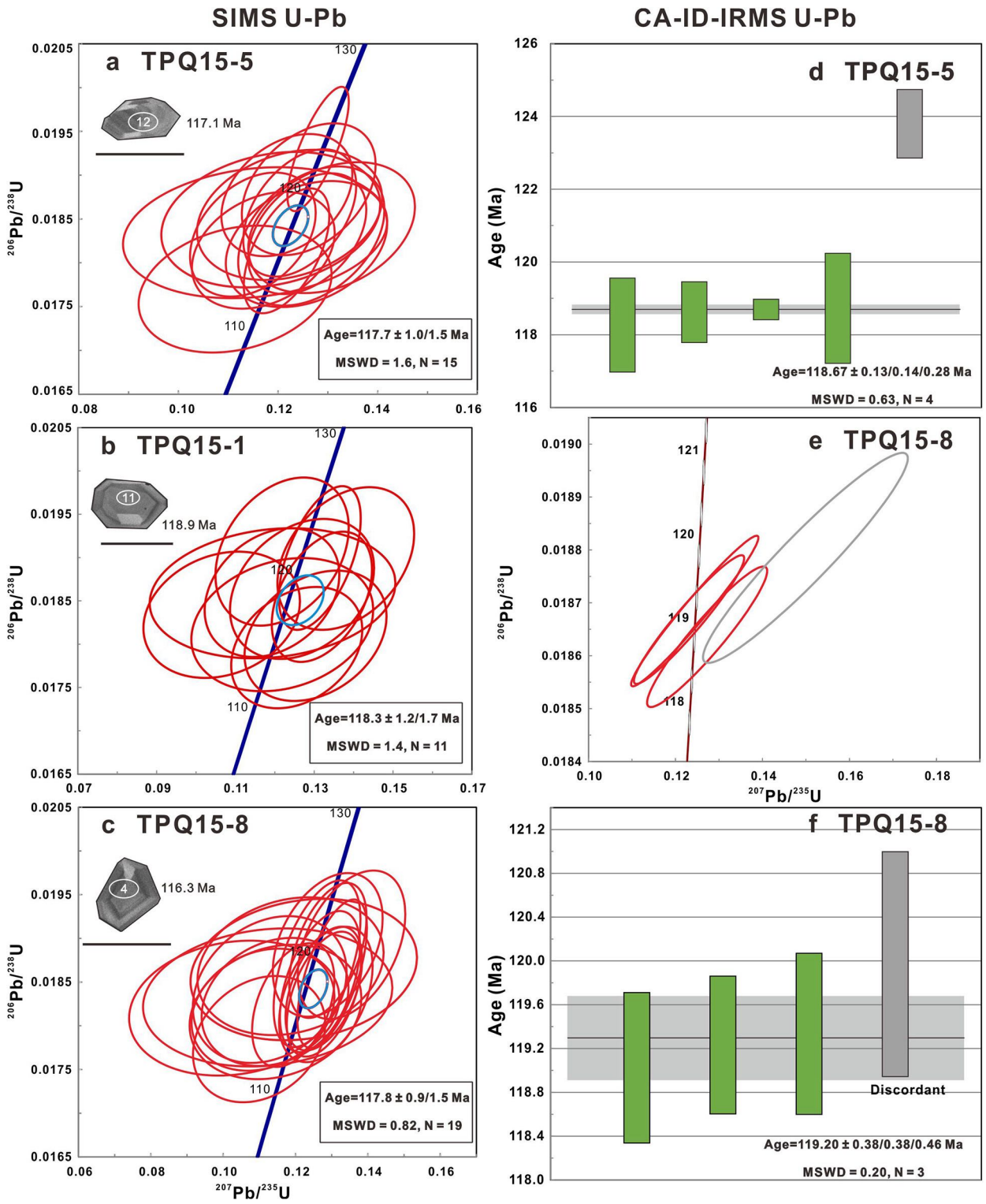

Fig. 4. SIMS U-Pb concordia age plots for zircons from the samples TPQ15–5 (a), TPQ15–1 (b), and TPQ15–8 (c), respectively. Ranked-age (d and f) and concordia age (e) plots show the results from analyzed samples by CA-ID-IRMS. See Fig. 1c and d for positions for the samples. Data-point error ellipses are 2σ level.

5. Discussion

5.1. Temporal constraints on the "Moqi fossil bed" and its associated Moqi Fauna

The two tuff samples, TPQ15–5 and TPQ15–1, were collected from tuff layers interbedded with the fossil-bearing layers where many frogs, salamanders, and other vertebrates were recovered and away from the baked layer, thus excluding the possibility of influence of the later geologic and thermal resetting events. The data indicate that these zircons are of volcanic origin and show no signs of sedimentary reworking or thermal resetting based on appearance of the layers and zircons and consistency of the U-Pb chronological results. The samples were successfully analyzed by SIMS U-Pb zircon dating method, yielding

weighted mean $^{206}Pb/^{238}U$ ages of 117.7 ± 1.0/1.5 Ma for sample TPQ15–5 and 118.3 ± 1.3/1.7 Ma for sample TPQ15–1 (Figs. 1c, 4, 5a), respectively. Considering the accuracy of the SIMS U-Pb dating method (Li et al., 2015a; Schaltegger et al., 2015) and the close positions of two dated samples of the Gezidong section, the two tuff layers yield indistinguishable ages. The sample TPQ15–8 from the Jiaxikou section (Figs. 1d, 4, 5a) yields a weighted mean $^{206}Pb/^{238}U$ age of 117.8 ± 0.9/1.5 Ma by SIMS U-Pb zircon analyses.

The samples TPQ15–5 and TPQ15–8 were further analyzed by CA-ID-IRMS U-Pb zircon dating methods, yielding weighted mean $^{206}Pb/^{238}U$ ages of 118.67 ± 0.13/0.14/0.28 Ma and 119.20 ± 0.38/0.38/0.46 Ma, respectively. The SIMS ages are consistent with the higher precision CA-ID-IRMS age of three tuff samples, indicating good reproducibility (accuracy). Furthermore, intercalibration among U-Pb zircon geochronologic laboratories here is aimed to yield more accurate and precise ages.

Accordingly, the ages of fossil-bearing layers from the Gezidong and Jiaxikou fossil localities are dated between 119.20 ± 0.38 Ma and 118.67 ± 0.13 Ma, respectively, corresponding to the Aptian Stage of the Early Cretaceous (Gale et al., 2020). The results are significantly younger and more precise than the LA-ICP-MS zircon age (121.2 ± 0.8 Ma) for the tuff reported by Wang et al. (2019). However, the assigned uncertainty of <1% is currently unrealistic for LA-ICP-MS data and is estimated to be approximately 4% (2RSD) (Li et al., 2015a; Schaltegger et al., 2015; Horstwood et al., 2016). Therefore, the date of Wang et al. (2019) could have high 2σ analytical uncertainties on individual U-Pb analyses that ranged from ±3 to ±11 Ma.

These two high-precision CA-ID-IRMS U-Pb ages provide temporal constraints on the Moqi fossil bed, as well as the Moqi Fauna, from 118.76 Ma to 119.20 Ma, refuting the previous proposal that the Moqi fossil bed at the Gezidong and Jiaxikou sections are temporally equivalent to the Yixian Formation in the Yanliao area (Jia and Gao, 2016;

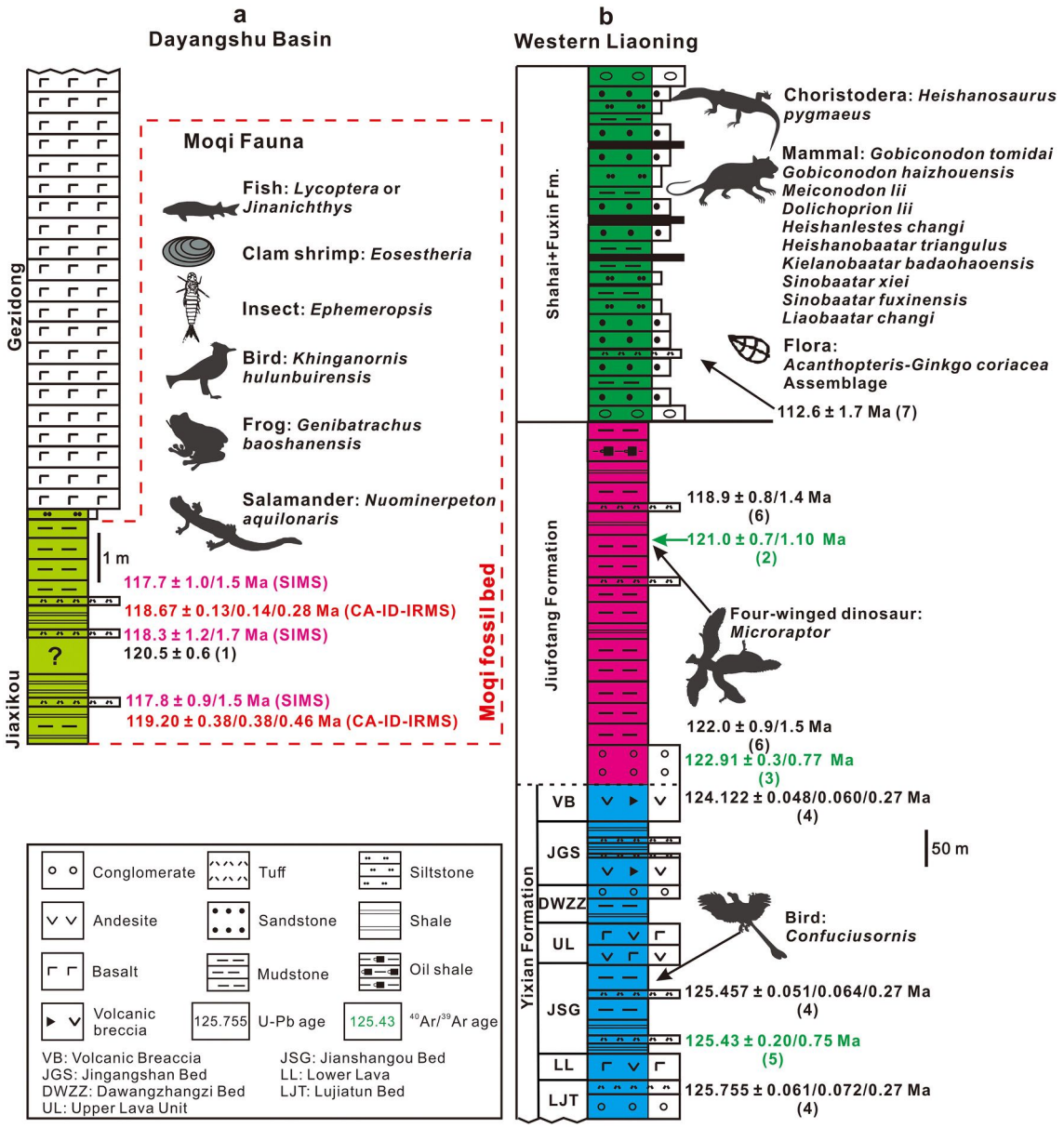

Fig. 5. Interregional correlation of the Moqi fossil bed of the Gezidong and Jiaxikou localities in the Dayangshu Basin to the strata from western Liaoning. Chronostratigraphy of the Dayangshu Basin (a) and western Liaoning (b), modified after Zhou et al. (2003, 2021). Sample positions and ages are indicated: (1) Wang et al., 2019; (2) He et al., 2004; (3) Chang et al., 2009; (4) Zhong et al., 2021; (5) Swisher et al., 1999; (6) Yu et al., 2021; (7) Xu et al., 2022. Vertebrate and plant fossils of the Jehol and Fuxin biotas are from Zhou et al., 2003; Xu et al., 2003; Kusuhashi et al., 2009a, 2009b, 2010, 2016, 2020; Deng et al., 2012; Dong et al., 2020.

Gao and Chen, 2017; Wang et al., 2019; Wang et al., 2021a). The new geochronology of the Moqi fossil bed could further allow for the valid correlation with the terrestrial volcanic-sedimentary sequences in adjacent areas and its paleontological comparison of the Cretaceous Jehol and Fuxin biotas in the Yanliao area.

The Songliao Basin is one of the largest Cretaceous continental rift basins in the world, which is located southeast to the Dayangshu Basin. The two basins were connected and became one basin when the first Member of the Nenjiang Formation was deposited (~85–83 Ma, Yu et al., 2019). Continuous high-resolution Cretaceous terrestrial geological records have been obtained from the Cretaceous Continental Scientific Drilling (hereafter termed CCSD-SK) Project in the Songliao Basin, providing a unique opportunity to understand the nature of terrestrial processes and their relationships with global geological and paleoenvironmental processes during the Cretaceous Period. The LA-ICP-MS U-Pb age of 118.2 ± 1.5 Ma at 5958.62 m (Liu et al., 2021) and the SIMS U-Pb age of 113.9 ± 0.9 Ma at 3961 m (Yu et al., 2020) of the CCSD-SK-II, constrained temporally the Shahezi Formation in the Songliao Basin. Therefore, the Moqi fossil bed in this study can be readily correlated to the lower part of the Shahezi Formation in the Songliao Basin, if dating uncertainty was considered.

Intense geochronologic studies have been conducted to constrain the age of the Lower Cretaceous successions in the Yanliao area, especially the Huajiying, Dabeigou, Dadianzi formations in northern Hebei, Yixian, Jiufotang, and Shahai formations in the western Liaoning where the important terrestrial biotas come from. The Huajiying (equivalent to the Dabeigou and Dadianzi formations in the Luanping Basin, Yu et al., 2022) and Yixian formations have been recently precisely dated between 135.4 Ma to 124.122 Ma (He et al., 2006; Yang et al., 2020; Zhong et al., 2021).

$^{40}Ar/^{39}Ar$ ages of 120.3 ± 0.7 Ma (recalculated to 121.0 ± 0.7 (Y)/1.1 (Z)) Ma, using the new decay constants and standard age (Min et al., 2000; Kuiper et al., 2008), for the Jiufotang Formation at the Shangheshou section, western Liaoning has been given (Fig. 5b, He et al., 2004). Most recently, the Jiufotang Formation of the Jianchang Basin, western Liaoning was precisely dated between 123 and 119 Ma by SIMS U-Pb zircon dating (Yu et al., 2021). And a LA-ICP-MS zircon U-Pb date, 112.6 ± 1.7 Ma, was made from the tuffaceous claystone of the upper part of Shahai Formation in Fuxin City, western Liaoning (Xu et al., 2022). At this point, we cannot rule out nor confirm if there is a relation between the Moqi fauna and the late Jehol Biota of the Jiufotang Formation. Therefore, the Moqi fossil bed is readily correlated to the uppermost Jiufotang Formation.

5.2. Comparison with other Early Cretaceous terrestrial biotas in Northeast China

Early Cretaceous fresh-water biotas in northeastern China, such as the Jehol and Fuxin biotas, are of great interest because of their high diversity and their important roles to understand the evolutionary history of many Mesozoic taxa (e.g., Wan et al., 2013; Wan et al., 2017; Xi et al., 2019; Zhou et al., 2021).

The appearance of a component of the *Eosestheria* fauna (clam shrimp), *Ephemeropsis* (insect), and possible *Lycoptera* or *Jinanichthy* (fish) in the Moqi Fauna suggests that a potential relation between the Moqi Fauna and the well-known Jehol Biota in the Yanliao area (Fig. 1, Chen, 1988; Zhou et al., 2003; Pan et al., 2013; Zhou, 2014). However, the poor definition of Jehol Biota based on the EEL assemblage gets in the way. As Pan et al. (2013) argued, the EEL assemblage cannot sufficiently represent the Jehol Biota, and only the Yixian Formation (corresponding to the middle stage of the Jehol Biota) yields the full set of the EEL (see section 3.1). Furthermore, the appearance of the so-called EEL assemblage in Moqi localities needs to be ascertained. For example, the taxonomy and composition of the *Eoestheria* fauna is still under revision (Hethke et al., 2018), making the comparison across different regions ambiguous. A detailed study on the abundant conchostracans from the Moqi localities is also lacking to reach a ground conclusion on the taxonomy of Moqi conchostracans.

Furthermore, the vertebrate species were not well shared by the Moqi Fauna and the Jehol Biota, except the rare fishes. The Moqi frogs are more advanced than the common Jehol ones (*Liaobatrachus* spp., Dong et al., 2013), which were recovered from the Yixian Formation. Moqi frogs are, in the view of evolutionary stages, closer to the frog material from the Jiufotang Formation by their undilated sacral urostyles and longer hindlimbs although the Jiufotang frogs are either juvenile individuals (Wang et al., 2007) or preserved relatively poorly (Dong, 2012). The Moqi salamander *Noumiperton* was recently recovered as the sister taxon of the only Jiufotang salamander *Liaoxitriton zhongjiani* within Panhynobia (stem Hynobiidae plus crown Hynobiidae) (Jia et al., 2021), but it should be noted that Panhynobia includes salamander species from Yanliao Biota, all stages of Jehol Biota, and Moqi Fauna, as well as extant ones. The bird *Khinganornis hulunbuirensis* is phylogenetically closest to the Jiufotang *Changzuiornis* and *Iteravis* (Wang et al., 2021b). The fact that the Moqi vertebrate components are phylogenetically or systematically related to the corresponding taxa of Jehol Biota does not suggest the vertebrates from Moqi localities are part of Jehol Biota. Moreover, Jehol Biota is much more diverse than the Moqi Fauna, with dozens of feathered dinosaurs, various birds, and primitive mammals. To further understand the nature of the Moqi Fauna and its relationship with the Jehol Biota, more and better fossil materials are needed.

Another diverse terrestrial biota from the Early Cretaceous of Northeast China is the Fuxin Biota of a slightly younger age (Xu et al., 2022). However, partly due to the biases in the devoted efforts, Fuxin Biota is represented mainly by disarticulated jaws and teeth of mammals (Kusuhashi et al., 2009a, 2009b, 2010, 2016, 2020; Wang et al., 2018a). There were some fishes (Jin, 1996) and dinosaur teeth and eggs (Amiot et al., 2010), as well as a lizard (*Teilhardosaurus*) and a choristoderan (*Heishanosaurus*), reported from the Fuxin Biota (Shikama, 1947; Dong et al., 2020). The fish taxon *Jinanichthys* could be possibly shared by the Moqi Fauna and Fuxin Biota, and otherwise the Moqi Fauna is distinct from the Fuxin Biota, as there is no mammal material as far as we know from the Moqi fauna, and the Moqi lizard material is clearly not related closely with *Teilhardosaurus*, by the body size and tooth morphology.

Taken the chronology and paleontology all together, the Moqi Fauna is now better treated as a separate fauna from Jehol Biota but somehow linked to the latter, and it is also distinct from the Fuxin Biota. As more and more fossils are coming out from the Moqi fossil bed, the Moqi Fauna shows more and more significance not only in the evolutionary history of several important vertebrate clades such as amphibians and birds, but also in understanding the spatiotemporal distribution, diversity, and pattern of radiation of the Early Cretaceous terrestrial biome in northeastern China (Zhou et al., 2021). This new Fauna will eventually help to elucidate the evolutionary history of the Early Cretaceous terrestrial biotas in East Asia.

6. Conclusions

The new fossil-bearing horizons at the Gezidong and Jiaxikou localities, eastern Inner Mongolia, are referred to as Moqi fossil bed and yield a diverse fossil assemblage coined as “Moqi Fauna” in this study. SIMS and CA-ID-IRMS zircon U-Pb geochronology of the Moqi fossil bed, demonstrates its ages between 119.20–118.67 Ma, and constrains the age of the Moqi Fauna of the Gezidong and Jiaxikou sections to the Aptian Stage of the Early Cretaceous. The Moqi Fauna will eventually help to elucidate the evolutionary history of the Early Cretaceous terrestrial biotas in East Asia as well as the evolutionary process of the Early Cretaceous terrestrial ecosystem. Comprehensive work on the geology and taphonomy of the Moqi Fossil bed and the paleontology and paleogeography of the Moqi Fauna are in urgent need.

Declaration of Competing Interest

None.

Acknowledgements

We are grateful to the journal editor Dr. Howard Falcon-Lang and three anonymous reviewers for their insightful and constructive comments. We thank Drs. Zhonghe Zhou, Rixiang Zhu, Qingren Meng, Xiaolin Wang, Gang Li, Xiaobo Li, Xiao Teng, Yufen Rong, and Lu Li for constructive suggestions and helpful discussions. We are grateful to Xiaobo Li, Lu Li, and Shaoguang Zhang for field assistance. We thank Qiuli Li, Xiaoping Xia, Qing Yang, Zexian Cui for their support and advice during the SIMS zircon U-Pb analysis. This work was supported by the National Natural Science Foundation of China (Grant No. 41688103), the Strategic Priority Program (B) of the Chinese Academy of Sciences (Grant No. XDB18000000). This paper is a contribution to the IGCP Project 679.

Appendix A. Supplementary data

Supplementary data to this article can be found online at https://doi.org/10.1016/j.palaeo.2021.110824.

References

Albarède, F., Albalat, E., Télouk, P., 2015. Instrumental isotope fractionation in multiple-collector icp-ms. J. Anal. At. Spectrom. 30 (8), 1736–1742. https://doi.org/10.1039/C5JA00188A.

Amiot, R., Kusuhashi, N., Xu, X., Wang, Y., 2010. Isolated dinosaur teeth from the lower cretaceous Shahai and Fuxin formations of northeastern China. J. Asian Earth Sci. 39 (5), 347–358. https://doi.org/10.1016/j.jseaes.2010.04.017.

Chang, M.M., Chen, P.J., Wang, Y.Q., Wang, Y., Miao, D.S., 2003. The Jehol Biota: The Emergence of Feathered Dinosaurs, Beaked Birds and Flowering Plants. Shanghai Scientific & Technical Publishers, Shanghai, China, pp. 11–18.

Chang, S.C., Zhang, H.C., Renne, P.R., Fang, Y., 2009. High-precision 40Ar/39Ar age for the Jehol Biota. Palaeogeograp. Palaeoclimatol. Palaeoecol. 280, 94–104. https://doi.org/10.1016/j.palaeo.2009.06.021.

Chen, P.J., 1988. Distribution and migration of Jehol fauna with reference to non-marine Jurassic/Cretaceous boundary in China. Acta Palaoentol. Sin. 27, 659–683 (in Chinese with English abstract).

Chiang, H.-W., Lu, Y., Wang, X., Lin, K., Liu, X., 2019. Optimizing MC-ICP-MS with SEM protocols for determination of U and Th isotope ratios and ^{230}Th ages in carbonates. Quat. Geochronol. 50, 75–90. https://doi.org/10.1016/j.quageo.2018.10.003.

Crowley, J.L., Schoene, B., Bowring, S.A., 2007. U-Pb dating of zircon in the Bishop Tuff at the millennial scale. Geology 35 (12), 1123–1126. https://doi.org/10.1130/G24017A.1.

Deng, S., Lu, Y., Fan, R., Li, X., Fang, L., Liu, L., 2012. Cretaceous floras and biostratigraphy of China. J. Stratigr. 36, 241–265.

Deng, C.L., He, H.Y., Pan, Y.X., Zhu, R.X., 2013. Chronology of the terrestrial Upper cretaceous in the Songliao Basin, Northeast Asia. Palaeogeogr. Palaeoclimatol. Palaeoecol. 385, 44–54. https://doi.org/10.1016/j.palaeo.2012.07.028.

Deng, C.Z., Sun, D.Y., Ping, X.Q., Huang, H., Zhang, L.D., Lu, S., 2019. Geochemistry of Early Cretaceous volcanic rocks in the northeastern Great Xing'an Range, Northeast China and implication for geodynamic setting. Int. Geol. Rev. 61 (13), 1594–1612. https://doi.org/10.1080/00206814.2018.1528481.

Ding, Q.H., Chen, S.W., Shang, L., Li, Y.F., Wang, J., 2014. New understanding of the Lower Cretaceous Longjiang Formation in the eastern Daxinganling region. Geol. Resour. 23, 215–234 (in Chinese with English abstract).

Dong, L.P., 2012. Restudy on the Anurans from the Jehol Biota (pp. 1–83),. Master thesis. Graduate School of Chinese Academy of Sciences (in Chinese).

Dong, L.P., Rocek, Z., Wang, Y., Jones, M.E.H., 2013. Anurans from the Lower Cretaceous Jehol Group of Western Liaoning, China. PLoS One 8, e69723. https://doi.org/10.1371/journal.pone.0069723.

Dong, L., Matsumoto, R., Kusuhashi, N., Wang, Y., Wang, Y., Evans, S.E., 2020. A new choristodere (Reptilia: Choristodera) from an Aptian–Albian coal deposit in China. J. Syst. Palaeontol. 18 (15), 1223–1242. https://doi.org/10.1080/14772019.2020.1749147.

Du, B.Y., Liu, Y.W., Zhao, M.S., Zhang, T.A., Zhao, Y.S., Feng, Z.Q., Zhen, M., Liu, Y.Q., Luo, J.X., 2018. Determination of the Early Cretaceous volcanic strata in eastern Jagdaqi, Daxinganling mountains. Geol. Resour. 27, 317–323 (in Chinese with English abstract).

Evans, S.E., Wang, Y., 2012. New material of the Early Cretaceous lizard *Yabeinosaurus* from China. Cretac. Res. 34, 48–60. https://doi.org/10.1016/j.cretres.2011.10.004.

Gale, A.S., Mutterlose, J., Batenburg, S., Gradstein, F.M., Agterberg, F.P., Ogg, J.G., Petrizzo, M.R., 2020. The Cretaceous Period. In: Gradstein, F.M., Ogg, J.G., Ogg, G. M. (Eds.), Geologic Time Scale 2020. Elsevier, Amsterdam, The Netherlands, pp. 1023–1086.

Gao, K.Q., Chen, J.Y., 2017. A new crown-group frog (Amphibia: Anura) from the Early Cretaceous of northeastern Inner Mongolia, China. Am. Mus. Novit. 3876, 1–39. https://doi.org/10.1206/3876.1.

Guo, H.Y., Sun, D.Y., Sun, R.J., Guo, J., Yang, D.G., Jing, H.X., 2015. Chronology and geochemistry of Mesozoic volcanic rocks from southeastern Mohe Basin. Global Geol. 34, 55–66 (in Chinese with English abstract).

HBGMR (Heilongjiang Bureau of Geology and Mineral Resources), 1993. Regional Geology of Heilongjiang Province (pp. 192–216). Geological Publishing House, Beijing, China (in Chinese).

HBGMR (Heilongjiang Bureau of Geology and Mineral Resources), 1997. Lithography in Heilongjiang Province (pp. 1–344). China University of Geosciences Press, Wuhan, China (in Chinese).

He, H.Y., Wang, X.L., Zhou, Z.H., Wang, F., Boven, A., Shi, G.H., Zhu, R.X., 2004. Timing of the Jiufotang Formation (Jehol Group) in Liaoning, northeastern China, and its implications. Geophys. Res. Lett. 31, L12605. https://doi.org/10.1029/2004GL019790.

He, H.Y., Wang, X.L., Jin, F., Zhou, Z.H., Wang, F.Y., Yang, L.K., Ding, X., Boven, A., Zhu, R.X., 2006. The ^{40}Ar/^{39}Ar dating of the early Jehol biota from Fengning, Hebei Province, northern China. Geochem. Geophys. Geosyst. 7 (4) https://doi.org/10.1029/2005GC001083.

He, H.Y., Deng, C.L., Wang, P.J., Pan, Y.X., Zhu, R.X., 2012. Toward age determination of the termination of the Cretaceous normal superchron. Geochem. Geophys. Geosyst. 13, Q02002. https://doi.org/10.1029/2011GC003901.

Hethke, M., Fursich, F.T., Morton, J.D., Jiang, B.Y., 2018. Analysis of morphological variability in the clam shrimp *Eosestheria middendorfii* (Crustacea, Spinicaudata) from the Lower Cretaceous of China, and its implications for spinicaudatan taxonomy. Papers Palaeontol. 4, 21–53. https://doi.org/10.1002/spp2.1096.

Hiess, J., Condon, D.J., McLean, N., Noble, S.R., 2012. ^{238}U/^{235}U systematics in terrestrial uranium-bearing minerals. Science 335 (6076), 1610–1614. https://doi.org/10.1126/science.1215507.

Horstwood, M.S., Košler, J., Gehrels, G., Jackson, S.E., McLean, N.M., Paton, C., Pearson, N.J., Sircombe, K., Sylvester, P., Vermeesch, P., Bowring, J.F., Condon, D.J., Schoene, B., 2016. Community-derived standards for LA-ICP-MS U-(Th-) Pb geochronology–uncertainty propagation, age interpretation and data reporting. Geostand. Geoanal. Res. 40 (3), 311–332. https://doi.org/10.1111/j.1751-908X.2016.00379.x.

Hu, Y.M., Meng, J., Wang, Y.Q., Li, C.K., 2005. Large Mesozoic mammals fed on young dinosaurs. Nature 433 (7022), 49–52. https://doi.org/10.1038/nature03102.

Huyskens, M.H., Iizuka, T., Amelin, Y., 2012. Evaluation of colloidal silicagels for lead isotopic measurements using thermal ionisation mass spectrometry. J. Anal. At. Spectrom. 27 (9), 1439–1446. https://doi.org/10.1039/C2JA30083D.

Huyskens, M.H., Zink, S., Amelin, Y., 2016. Evaluation of temperature-time conditions for the chemical abrasion treatment of single zircons for U–Pb geochronology. Chem. Geol. 438, 25–35. https://doi.org/10.1016/j.chemgeo.2016.05.013.

IMBGMR (Inner Mongolian Bureau of Geology and Mineral Resources), 1991. Regional Geology of Inner Mongolia (Pp. 237–270). Geological Publishing House, Beijing, China (in Chinese).

IMBGMR (Inner Mongolian Bureau of Geology and Mineral Resources), 1996. Lithography in Inner Mongolia Autonomous Region (pp. 1–344). China University of Geosciences Press, Wuhan, China (in Chinese).

Jaffey, A.H., Flynn, K.F., Glendenin, L.E., Bentley, W.T., Essling, A.M., 1971. Precision measurement of half-lives and specific activities of ^{235}U and ^{238}U. Phys. Rev. C 4 (5), 1889. https://doi.org/10.1103/PhysRevC.4.1889.

Jia, J., Gao, K.Q., 2016. A new hynobiid-like salamander (Amphibia, Urodela) from Inner Mongolia, China, Provides a rare case study of developmental features in an Early Cretaceous fossil urodele. Peer J. 4, e2499 https://doi.org/10.7717/peerj.2499.

Jia, J., Anderson, J.S., Gao, K.Q., 2021. Middle Jurassic stem hynobiid from China shed light on the evolution of basal salamanders. IScience 102744. https://doi.org/10.1016/j.isci.2021.102744.

Jiang, B.Y., Harlow, G.E., Wohletz, K., Zhou, Z.H., Meng, J., 2014. New evidence suggests pyroclastic flows are responsible for the remarkable preservation of the Jehol biota. Nat. Commun. 5 (1), 1–7. https://doi.org/10.1038/ncomms4151 (2014).

Jin, F., 1996. New advances in the late Mesozoic stratigraphic research of western Liaoning, China. Vertebrata Palasiatica 34, 102–122 (in Chinese with English abstract).

Kuiper, K.F., Deino, A., Hilgen, F.J., Krijgsman, W., Renne, P.R., Wijbrans, A.J., 2008. Synchronizing rock clocks of Earth history. Science 320, 500–504. https://doi.org/10.1126/science.1154339.

Kusuhashi, N., Hu, Y.M., Wang, Y.Q., Hirasawa, S., Matsuoka, H., 2009a. New triconodontids (Mammalia) from the Lower Cretaceous Shahai and Fuxin formations, northeastern China. Geobios 42, 765–781. https://doi.org/10.1016/j.geobios.2009.06.003.

Kusuhashi, N., Hu, Y.M., Wang, Y.Q., Setoguchi, T., Matsuoka, H., 2009b. Two eobaatarid (Multituberculata; Mammalia) genera from the Lower Cretaceous Shahai and Fuxin Formations, northeastern. J. Vertebr. Paleontol. 29, 1264–1288. https://doi.org/10.1671/039.029.0433.

Kusuhashi, N., Hu, Y.M., Wang, Y.Q., Setoguchi, T., Matsuoka, H., 2010. New multituberculate mammals from the Lower Cretaceous (Shahai and Fuxin formations), northeastern China. J. Vertebr. Paleontol. 30, 1501–1514. https://doi.org/10.1080/02724634.2010.501435.

Kusuhashi, N., Wang, Y.Q., Li, C.K., Jin, X., 2016. Two new species of *Gobiconodon* (Mammalia, Eutriconodonta, Gobiconodontidae) from the Lower Cretaceous Shahai and Fuxin formations, northeastern China. Hist. Biol. 28, 14–26. https://doi.org/10.1080/08912963.2014.977881.

Kusuhashi, N., Wang, Y.Q., Jin, X., 2020. A new eobaatarid multituberculate (Mammalia) from the Lower Cretaceous Fuxin formation, Fuxin-Jinzhou Basin, Liaoning, Northeastern China. J. Mamm. Evol. 27 (4), 605–623. https://doi.org/10.1007/s10914-019-09481-w.

Li, X.B., 2010. The Early Cretaceous Jehol Biota and Stratigraphy in the Northern Great Xing'an Range and Adjacent Areas. Jilin University, pp. 1–174. PhD. Thesis.

Li, X.B., Reisz, R., 2020. The stratigraphy and paleoenvironment of a '*Lycoptera* Bed'site in eastern Inner Mongolia, China: correlation with the fossiliferous Lower Cretaceous strata in western Liaoning. Palaeogeogr. Palaeoclimatol. Palaeoecol. 559, 109951 https://doi.org/10.1016/j.palaeo.2020.109951.

Li, G., Shen, Y.B., Batten, D.J., 2007. *Yanjiestheria*, *Yanshania* and the development of the *Eosestheria* conchostracan fauna of the Jehol Biota in China. Cretac. Res. 28, 225–234. https://doi.org/10.1016/j.cretres.2006.07.002.

Li, X.H., Liu, Y., Li, Q.L., Guo, C.H., Chamberlain, K.R., 2009. Precise determination of Phanerozoic zircon Pb/Pb age by multicollector SIMS without external standardization. Geochem. Geophys. Geosyst. 10, Q04010. https://doi.org/10.1029/2009GC002400.

Li, Q.L., Li, X.H., Liu, Y., Tang, G.Q., Yang, J.H., Zhu, W.G., 2010. Precise U–Pb and Pb–Pb dating of Phanerozoic baddeleyite by SIMS with oxygen flooding technique. J. Anal. At. Spectrom. 25, 1107. https://doi.org/10.1039/B923444F.

Li, X.H., Tang, G.Q., Guo, B., Yang, Y.H., Hou, K.J., Hu, Z.C., Li, Q.L., Liu, Y., Li, W.X., 2013. Qinghu zircon: a working reference for microbeam analysis of U-Pb age and Hf and O isotopes. Chin. Sci. Bull. 58, 1954–1961. https://doi.org/10.1007/s11434-013-5932-x.

Li, Y.F., Gao, X.Y., Bian, X.F., Chen, S.W., Ding, Q.H., 2013a. LA-ICP-MS zircon U-Pb dating and geochemical characteristics of the Mesozoic volcanic rocks from Longjiang basin in northern Da Hinggan Mountains and their geological implications. Geol. Bull. China 32, 1195–1211 (in Chinese with English abstract).

Li, Y.F., Bian, X.F., Gao, X.Y., Chen, S.W., Ding, Q.H., 2013b. Laser $^{40}Ar/^{39}Ar$ chronology of the Mesozoic volcanic rocks from Longjiang basin in northern Da Hinggan Mountains. Geol. Bull. China 32, 1212–1223 (in Chinese with English abstract).

Li, X.H., Liu, X.M., Liu, Y.S., Su, L., Sun, W.D., Huang, H.Q., Yi, K., 2015a. Accuracy of LA-ICPMS zircon U-Pb age determination: an inter-laboratory comparison. Sci. China Earth Sci. 58 (10), 1722–1730. https://doi.org/10.1007/s11430-015-5110-x.

Li, Y.F., Zhao, Y., Sun, C.L., Li, H.M., Chen, Y.J., 2015b. Chronological and geochemical characteristics of volcanic rocks from Early Cretaceous Longjiang Formation in Xinsheng area, Northern Heilongjiang. Global Geol. 34, 12–24 (in Chinese with English abstract).

Liao, S.Y., Huyskens, M.H., Yin, Q.Z., Schmitz, B., 2020. Absolute dating of the L-chondrite parent body breakup with high-precision U–Pb zircon geochronology from Ordovician limestone. Earth Planet. Sci. Lett. 547, 116442 https://doi.org/10.1016/j.epsl.2020.116442.

Liu, H.B., Wang, P.J., Gao, Y.F., Hou, H.S., Yin, Y.K., Li, H.H., Feng, Y.H., 2021. New data from ICDP borehole SK2 and its constraint on the beginning of the Lower Cretaceous Shahezi Formation in the Songliao Basin, NE China. Sci. Bull. 66, 411–413. https://doi.org/10.1016/j.scib.2020.12.002.

Mattinson, J.M., 2005. Zircon U-Pb chemical abrasion ("CA-TIMS") method: combined annealing and multi-step partial dissolution analysis for improved precision and accuracy of zircon ages. Chem. Geol. 220 (1–2), 47–66. https://doi.org/10.1016/j.chemgeo.2005.03.011.

Meng, Q.R., Zhou, Z.H., Zhu, R.X., Xu, Y.G., Guo, Z.T., 2021. Cretaceous basin evolution in Northeast Asia: Tectonic responses to the paleo-Pacific plate subduction. Natl. Sci. Rev. nwab088. https://doi.org/10.1093/nsr/nwab088.

Min, K., Mundil, R., Renne, P.R., Ludwig, K.R., 2000. A test for systematic errors in $^{40}Ar/^{39}Ar$ geochronology through comparison with U/Pb analysis of a 1.1-Ga rhyolite. Geochim. Cosmochim. Acta 64, 73–98. https://doi.org/10.1016/S0016-7037(99)00204-5.

Pan, Y.H., Sha, J.G., Zhou, Z.H., Fürsich, F.T., 2013. The Jehol Biota: definition and distribution of exceptionally preserved relicts of a continental Early Cretaceous ecosystem. Cretac. Res. 44, 30–38. https://doi.org/10.1016/j.cretres.2013.03.007.

Ren, J.Y., Tamaki, K., Li, S.T., Zhang, J.X., 2002. Late Mesozoic and Cenozoic rifting and its dynamic setting in Eastern China and adjacent areas. Tectonophysics 344, 175–205. https://doi.org/10.1016/S0040-1951(01)00271-2.

Roček, Z., Dong, L.P., Fabrezi, M., Rong, Y.F., Wang, Y., 2022. Carpus in Mesozoic anurans: the Early Cretaceous anuran *Genibatrachus* from northeastern China. Cretac. Res. 129, 104984 https://doi.org/10.1016/j.cretres.2021.104984.

Rogers, C.S., Hone, D.W., McNamara, M.E., Zhao, Q., Orr, P.J., Kearns, S.L., Benton, M.J., 2015. The Chinese Pompeii? Death and destruction of dinosaurs in the Early Cretaceous of Lujiatun, NE China. Palaeogeogr. Palaeoclimatol. Palaeoecol. 427, 89–99. https://doi.org/10.1016/j.palaeo.2015.03.037.

Schaltegger, U., Schmitt, A.K., Horstwood, M.S.A., 2015. U–Th–Pb zircon geochronology by ID-TIMS, SIMS, and laser ablation ICP-MS: recipes, interpretations, and opportunities. Chem. Geol. 402, 89–110. https://doi.org/10.1016/j.chemgeo.2015.02.028.

Schaltegger, U., Ovtcharova, M., Gaynor, S.P., Schoene, B., Wotzlaw, J.F., Davies, J.H., Farina, F., Greber, N.D., Szymanowski, D., Chelle-Michou, C., 2021. Long-term repeatability and interlaboratory reproducibility of high-precision ID-TIMS U-Pb geochronology. J. Anal. At. Spectrom. 36, 1466–1477. https://doi.org/10.1039/D1JA00116G.

Schmitz, M.D., Schoene, B., 2007. Derivation of isotope ratios, errors, and error correlations for U-Pb geochronology using ^{205}Pb-^{235}U-(^{233}U)-spiked isotope dilution thermal ionization mass spectrometric data. Geochem. Geophys. Geosyst. 8 (8) https://doi.org/10.1029/2006GC001492.

Shikama, T., 1947. *Teihardosaurus* and *Endotherium*, new Jurassic Reptilia and Mammalia from the Husin Coal-Field, South Manchuria. Proc. Jpn Acad. 23, 76–84. https://doi.org/10.2183/pjab1945.23.76.

Sláma, J., Košler, J., Condon, D.J., Crowley, J.L., Gerdes, A., Hanchar, J.M., Horstwood, M.S.A., Morris, G.A., Nasdala, L., Norberg, N., Schaltegger, U., Schoene, B., Tubrett, M.N., Whitehouse, M.J., 2008. Plešovice zircon—a new natural reference material for U–Pb and Hf isotopic microanalysis. Chem. Geol. 249 (1–2), 1–35. https://doi.org/10.1016/j.chemgeo.2007.11.005.

Sun, G., Dilcher, D.L., Zheng, S.L., Zhou, Z.H., 1998. In search of the first flower: a Jurassic angiosperm, *Archaefructus*, from Northeast China. Science 282 (5394), 1692–1695. https://doi.org/10.1126/science.282.5394.1692.

Sun, G., Ji, Q., Dilcher, D.L., Zheng, S.L., Nixon, K.C., Wang, X.F., 2002. Archaefructaceae, a new basal angiosperm family. Science 296 (5569), 899–904. https://doi.org/10.1126/science.1069439.

Sun, L., Wang, C.L., Bian, X.F., 2020. A new palynological assemblage from the Nenjiang Formation of Dayangshu Basin, and its geological implication. Acta Geol. Sin. Engl. Ed. 94 (1), 198–199. https://doi.org/10.1111/1755-6724.14416.

Swisher, C.C., Wang, Y.Q., Wang, X.L., Xu, X., Wang, Y., 1999. Cretaceous age for the feathered dinosaurs of Liaoning, China. Nature 400, 58–61. https://doi.org/10.1038/21872.

Verbruggen, A., et al., 2008. Preparation and Certification of IRMM-3636, IRMM-3636a and IRMM-3636b. OPOCE (24pp).

Villa, I.M., Bonardi, M.L., De Bièvre, P., Holden, N.E., Renne, P.R., 2016. IUPAC-IUGS status report on the half-lives of ^{238}U, ^{235}U and ^{234}U. Geochim. Cosmochim. Acta 172, 387–392. https://doi.org/10.1016/j.gca.2015.10.011.

von Quadt, A., Wotzlaw, J.F., Buret, Y., Large, S.J., Peytcheva, I., Trinquier, A., 2016. High-precision zircon U/Pb geochronology by ID-TIMS using new 10^{13} ohm resistors. J. Anal. At. Spectrom. 31 (3), 658–665. https://doi.org/10.1039/C5JA00457H.

Wan, X.Q., Zhao, J., Scott, R.W., Wang, P.J., Feng, Z.H., Huang, Q.H., Xi, D.P., 2013. Late Cretaceous stratigraphy, Songliao Basin, NE China: SK1 cores. Palaeogeogr. Palaeoclimatol. Palaeoecol. 385, 31–43. https://doi.org/10.1016/j.palaeo.2012.10.024.

Wan, X.Q., Wu, H.C., Xi, D.P., Liu, M.Y., Qin, Z.H., 2017. Terrestrial biota and climate during Cretaceous greenhouse in NE China. Earth Sci. Front. 24 (1), 18–31 (in Chinese with English abstract). https://doi.org/10.1016/10.13745/j.esf.2017.01.002.

Wang, Y., Evans, S.E., 2006. Advances in the study of fossil amphibians and squamates from China: the past fifteen years. Vertebrata PalAsiatica 44 (1), 60–73. https://doi.org/10.19615/j.cnki.1000-3118.2006.01.004.

Wang, Y.Q., Su, Y.Z., Liu, E.Y., 1997. Regional Stratigraphy of the Northeast Region. China University of Geosciences Press. (in Chinese), Wuhan, China, pp. 76–113.

Wang, Y., Jones, M.E.H., Evans, S.E., 2007. A juvenile anuran from the Lower Cretaceous Jiufotang Formation, Liaoning, China. Cretac. Res. 28, 235–244. https://doi.org/10.1016/j.cretres.2006.07.003.

Wang, C.S., Feng, Z.Q., Zhang, L.M., Huang, Y.J., Cao, K., Wang, P.J., Zhao, B., 2013. Cretaceous paleogeography and paleoclimate and the setting of SKI borehole sites in Songliao Basin, Northeast China. Palaeogeogr. Palaeoclimatol. Palaeoecol. 385, 17–30. https://doi.org/10.1016/j.palaeo.2012.01.030.

Wang, L., Cheng, X.T., Li, W., Liu, S.Z., Wang, X.R., 2017a. A new species of Cretadromus from the Lower Cretaceous Guanghua Formation in the Da Hinggan Mountains, Inner Mongolia. Geol. China 44, 818–819 (in Chinese with English abstract).

Wang, S.S., Liu, J.Y., Ji, H.W., Lv, J., Zhou, S., Liu, J.L., 2017b. Geochronology and geochemistry of the andesite of Longjiang Formation in the Sandaowanzi gold deposit, Heilongjiang Province. Acta Petrol. Sin. 33 (8), 2604–2618 (in Chinese with English abstract).

Wang, X.R., Wang, L., Ji, Q., 2017c. First discovered diversified fossil locality of the Jehol Biota in the Greater Khingan Mountains, Inner Mongolia. Acta Geol. Sin. Engl. Ed. 91 (5), 1906–1907.

Wang, Y.Q., Kusuhashi, N., Jin, X., 2018a. Reappraisal of *Endotherium niinomii* Shikama, 1947, a eutherian mammal from the Lower Cretaceous Fuxin Formation, Fuxin-Jinzhou Basin, Liaoning, China. Vertebrata PalAsiatica 56, 180–192. https://doi.org/10.19615/j.cnki.1000-3118.180226.

Wang, M., Stidham, T.A., Zhou, Z.H., 2018b. A new clade of basal Early Cretaceous pygostylian birds and developmental plasticity of the avian shoulder girdle. Proc. Natl. Acad. Sci. 115 (42), 10708–10713. https://doi.org/10.1073/pnas.1812176115.

Wang, X.R., Ji, S., Wang, Y., 2019. First Zircon U-Pb Ages of the Pigeon Hill Fossil Locality of the Jehol Biota in the Greater Khingan Mountains, Inner Mongolia. Acta Geol. Sin. Engl. Ed. 93, 1142–1145. https://doi.org/10.1111/1755-6724.14348.

Wang, H.B., Meng, J., Wang, Y.Q., 2019a. Cretaceous fossil reveals a new pattern in mammalian middle ear evolution. Nature 576 (7785), 102–105. https://doi.org/10.1038/s41586-019-1792-0.

Wang, X.R., Cau, A., Kundrát, M., Chiappe, L.M., Ji, Q., Wang, Y., Li, T., Wu, W.H., 2021a. A new advanced ornithuromorph bird from Inner Mongolia documents the northernmost geographic distribution of the Jehol paleornithofauna in China. Hist. Biol. 33 (9), 1705–1717. https://doi.org/10.1080/08912963.2020.1731805.

Wang, M., Lloyd, G.T., Zhang, C., Zhou, Z.H., 2021b. The patterns and modes of the evolution of disparity in Mesozoic birds. Proc. R. Soc. B Biol. Sci. 288, 20203105. https://doi.org/10.1098/rspb.2020.3105.

Wu, F.Y., Sun, D.Y., Ge, W.C., Zhang, Y.B., Grant, M.L., Wilde, S.A., Jahn, B.M., 2011. Geochronology of the Phanerozoic granitoids in northeastern China. J. Asian Earth Sci. 41 (1), 1–30. https://doi.org/10.1016/j.jseaes.2010.11.014.

Xi, D.P., Wan, X.Q., Li, G.B., Li, G.B., 2019. Cretaceous integrative stratigraphy and timescale of China. Sci. China Earth Sci. 62, 256–286. https://doi.org/10.1007/s11430-017-9262-y.

Xing, L.D., Niu, K., Evans, S.E., 2019. Inter-amphibian predation in the Early Cretaceous of China. Sci. Rep. 9, 1–5. https://doi.org/10.1038/s41598-019-44247-7.

Xu, X., Norell, M.A., 2004. A new troodontid dinosaur from China with avian-like sleeping posture. Nature 431, 838–841. https://doi.org/10.1038/nature02898.

Xu, X., Zhou, Z.H., Wang, X.L., Kuang, X.W., Zhang, F.C., Du, X.K., 2003. Four-winged dinosaurs from China. Nature 421 (6921), 335–340. https://doi.org/10.1038/nature01342.

Xu, X., Zhou, Z.H., Wang, Y., Wang, M., 2020. Study on the Jehol Biota: recent advances and future prospects. Sci. China Earth Sci. 63 (6), 757–773. https://doi.org/10.1007/s11430-019-9509-3.

Xu, X.T., Shao, L.Y., Eriksson, K.A., Pang, B., Wang, S., Yang, C.X., Hou, H.H., 2022. Terrestrial records of the early Albian Ocean Anoxic Event: evidence from the Fuxin lacustrine basin, NE China. Geosci. Front. 13 (1), 101275 https://doi.org/10.1016/j.gsf.2021.101275.

Yang, S.H., He, H.Y., Jin, F., Zhang, F.C., Wu, Y.B., Yu, Z.Q., Li, Q.L., Wang, M., O'Connor, J.K., Deng, C.L., Zhu, R.X., Zhou, Z.H., 2020. The appearance and duration of the Jehol Biota: Constraint from SIMS U-Pb zircon dating for the Huajiying Formation in northern China. Proc. Natl. Acad. Sci. 117, 14299–14305. https://doi.org/10.1073/pnas.1918272117.

Yokoyama, T., Makishima, A., Nakamura, E., 2001. Precise analysis of $^{234}U/^{238}U$ ratio using UO_2^+ ion with thermal ionization mass spectrometry for natural samples. Chem. Geol. 181 (1), 1–12. https://doi.org/10.1016/S0009-2541(01)00270-4.

Yu, Z.Q., He, H.Y., Deng, C.L., Xi, D.P., Qin, Z.H., Wan, X.Q., Wang, C.S., Zhu, R.X., 2019. New geochronological constraints for the Upper Cretaceous Nenjiang Formation in the Songliao Basin, NE China. Cretac. Res. 102, 160–169. https://doi.org/10.1016/j.cretres.2019.05.006.

Yu, Z.Q., He, H.Y., Deng, C.L., Lu, K., Shen, Z.S., Li, Q.L., 2020. New SIMS U-Pb geochronology for the Shahezi Formation from CCSD-SK-IIe borehole in the Songliao Basin, NE China. Sci. Bull. 65 (13), 1049–1051. https://doi.org/10.1016/j.scib.2020.03.039.

Yu, Z.Q., Wang, M., Li, Y.J., Deng, C.L., He, H.Y., 2021. New geochronological constraints for the Lower Cretaceous Jiufotang Formation in Jianchang Basin, NE China, and their implications for the late Jehol Biota. Palaeogeogr. Palaeoclimatol. Palaeoecol. 583, 110657 https://doi.org/10.1016/j.palaeo.2021.110657.

Yu, Z.Q., Qin, Z.H., Xi, D.P., Deng, C.L., He, H.Y., Zhou, Z.H., 2022. New geochronology of the Lower Cretaceous in the Luanping Basin, northern Hebei: Age constraints on the development of early Jehol Biota. Palaeogeogr. Palaeoclimatol. Palaeoecol. 586C, 110768 https://doi.org/10.1016/j.palaeo.2021.110768.

Zhang, G., Wang, Y., Jones, M.E.H., Evans, S.E., 2009. A new Early Cretaceous salamander (*Regalerpeton weichangensis* gen. et sp. nov.) from the Huajiying Formation of northeastern China. Cretac. Res. 30, 551–558. https://doi.org/10.1016/j.cretres.2008.10.004.

Zhang, C., Wu, X.W., Zhang, Y.J., Guo, W., Quan, J.Y., 2017. LA-ICP-MS zircon U-Pb dating and geochemical characteristics of the pantellerite of Guanghua Formation from Longjiang Basin in northern Da Hinggan Mountains and their geological implications. Geol. Bull. China 36, 1531–1541 (in Chinese with English abstract).

Zhang, C., Wu, X.W., Zhang, Y.J., Guo, W., Quan, J.Y., 2018. Geochemistry and zircon LA- ICP- MS U- Pb age of volcanic rocks in Longjiang Formation of Longjiang basin. Geol. China 45 (3), 456–468 (in Chinese with English abstract).

Zhang, L.J., Chu, H., Wang, X., Han, G., Gao, F., 2020. New findings of the angiosperm-bearing strata in Ganhe, central Dayangshu Basin, Inner Mongolia, NE China. J. Stratigr. 44, 326–336 in Chinese with English abstract. 10.19839/j.cnki.dcxzz.2020.0024.

Zhong, Y.T., Huyskens, M.H., Yin, Q.Z., Wang, Y.Q., Ma, Q., Xu, Y.G., 2021. High-precision geochronological constraints on the duration of 'Dinosaurs Pompeii' and the Yixian Formation. Natl. Sci. Rev. 8 (6), nwab063. https://doi.org/10.1093/nsr/nwab063.

Zhou, Z.H., 2014. The Jehol Biota, an Early Cretaceous terrestrial Lagerstätte: new discoveries and implications. Natl. Sci. Rev. 1, 543–559. https://doi.org/10.1093/nsr/nwu055.

Zhou, Z.H., Wang, Y., 2017. Vertebrate assemblages of the Jurassic Yanliao Biota and the Early Cretaceous Jehol Biota: comparisons and implications. Palaeoworld 26 (2), 241–252. https://doi.org/10.1016/j.palwor.2017.01.002.

Zhou, Z.H., Barrett, P.M., Hilton, J., 2003. An exceptionally preserved Lower Cretaceous ecosystem. Nature 421, 807–814. https://doi.org/10.1038/nature01420.

Zhou, Z.H., Meng, Q.R., Zhu, R.X., Wang, M., 2021. Spatiotemporal evolution of the Jehol Biota: responses to the North China craton destruction in the Early Cretaceous. Proc. Natl. Acad. Sci. 118 (34), e2107859118 https://doi.org/10.1073/pnas.2107859118.